Bone vascular niche E-selectin induces mesenchymal–epithelial transition and Wnt activation in cancer cells to promote bone metastasis

Mark Esposito[1], Nandini Mondal[2,3,8], Todd M. Greco[1,8], Yong Wei[1], Chiara Spadazzi[4],
Song-Chang Lin[5], Hanqiu Zheng[1], Corey Cheung[1], John L. Magnani[6], Sue-Hwa Lin[5],
Ileana M. Cristea[1], Robert Sackstein[2,3,7] and Yibin Kang[1]*

How disseminated tumour cells engage specific stromal components in distant organs for survival and outgrowth is a critical but poorly understood step of the metastatic cascade. Previous studies have demonstrated the importance of the epithelial–mesenchymal transition in promoting the cancer stem cell properties needed for metastasis initiation, whereas the reverse process of mesenchymal–epithelial transition is required for metastatic outgrowth. Here we report that this paradoxical requirement for the simultaneous induction of both mesenchymal–epithelial transition and cancer stem cell traits in disseminated tumour cells is provided by bone vascular niche E-selectin, whose direct binding to cancer cells promotes bone metastasis by inducing mesenchymal–epithelial transition and activating Wnt signalling. E-selectin binding activity mediated by the α1-3 fucosyltransferases Fut3/Fut6 and Glg1 are instrumental to the formation of bone metastasis. These findings provide unique insights into the functional role of E-selectin as a component of the vascular niche critical for metastatic colonization in bone.

A critical gap in our understanding of cancer metastasis lies between the initial dissemination of circulating tumour cells to a secondary organ and their successful outgrowth to metastatic lesions[1,2]. Two molecular themes central to metastasis initiation have emerged from recent studies: cellular plasticity mediated by epithelial—mesenchymal and mesenchymal—epithelial transitions (EMT and MET, respectively)[3,4], and tumour–stromal niche interactions, which activate the properties of tumour-initiating or cancer stem cells through Wnt, Notch and other pathways[5,6]. Despite numerous studies, we do not yet understand how these programs interact to initiate metastasis.

The acquisition of mesenchymal traits through EMT has been shown to promote many pro-metastatic properties[7–9]. However, secondary metastatic tumours often match the epithelial state of the primary tumour[10] and studies have suggested a requirement for MET during metastatic colonization[3,11–14]. Thus, it has been proposed that sequential EMT–MET are needed for tumour cells to colonize a distant organ[3]. Yet this hypothesis does not explain the paradox of how MET induction and stem-cell identity coexist when essential stem- and metastasis-associated factors such as Sox2 are suppressed in an epithelial state[15,16]. Furthermore, the causes of these sequential epithelial–mesenchymal–epithelial transitions remain only half described; the inducers of EMT are well-studied[4] yet few inducers of MET are known.

For metastatic cells to colonize an organ, the inducers of MET must act in a context-dependent manner, which suggests that tumour–stromal interactions are instructive to MET. Clues from previous studies suggest that the bone vascular niche that hosts haematopoietic stem/progenitor cells (HSCs/HPCs) may contain such stromal signals, as this niche is co-opted by cancer cells during bone metastasis[17,18]. One factor essential to the function of the HSC/HPC vascular niche is endothelial selectin (E-selectin, Sele or CD62e). As originally defined, E-selectin functions to capture circulating leukocytes or tumour cells onto vascular endothelium under haemodynamic shear flow[19], yet leukocyte recruitment is not altered by the ablation of E-selectin[20]. Further studies have shown that E-selectin plays a critical role in the creation of the bone marrow vascular niche that drives haematopoiesis and engagement of E-selectin with its ligands on haematopoietic progenitor cells[21] leads to their proliferation[22].

Although it is known that certain tumour cells bind to E-selectin in vitro[19,23,24], genetic ablation of E-selectin has not been shown to affect metastasis in vivo; furthermore, our knowledge of the role of E-selectin receptor–ligand interactions in metastasis is incomplete. Here we report that Golgi glycoprotein 1 (Glg1 or E-selectin ligand 1) and glycoprotein E-selectin ligands created by the α1–3 fucosyltransferases 3 or 6 (Fut3/6) play key roles in mediating metastasis to bone by binding E-selectin, which induces a MET followed by stemness-enhancing Wnt signalling.

[1]Department of Molecular Biology, Princeton University, Princeton, NJ, USA. [2]Department of Dermatology and Harvard Skin Disease Research Center, Brigham and Women's Hospital, Harvard Medical School, Boston, MA, USA. [3]Program of Excellence in Glycosciences, Harvard Medical School, Boston, MA, USA. [4]Osteoncology and Rare Tumors Center, Istituto Scientifico Romagnolo per lo Studio e la Cura dei Tumori IRCCS, Meldola, Italy. [5]Department of Translational Molecular Pathology, The University of Texas MD Anderson Cancer Center, Houston, TX, USA. [6]Glycomimetics Inc., Gaithersburg, MD, USA. [7]Department of Medicine, Brigham and Women's Hospital, Harvard Medical School, Boston, MA, USA. [8]These authors contributed equally: Nandini Mondal, Todd M. Greco. *e-mail: ykang@princeton.edu
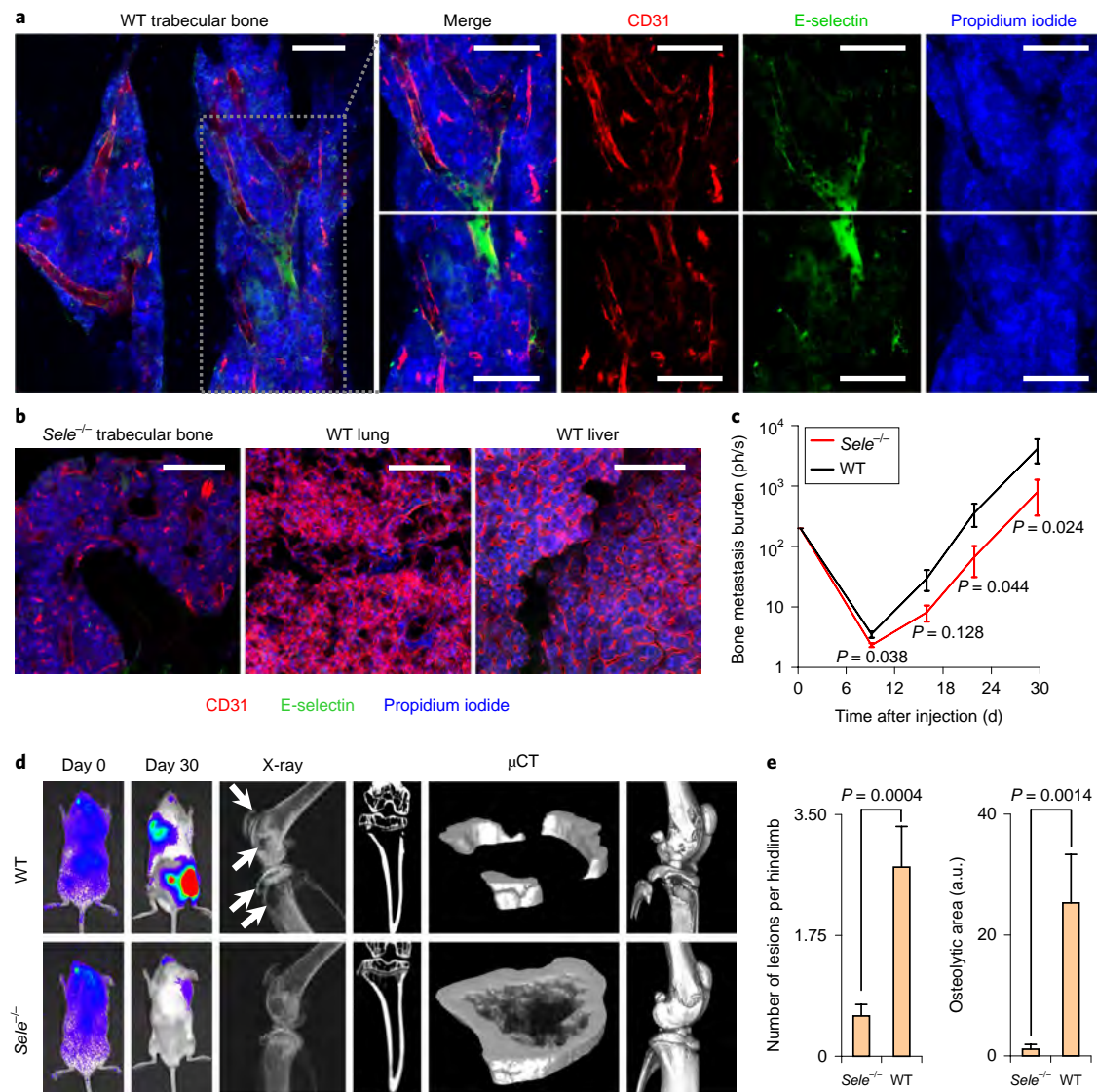
Fig. 1 | E-selectin is critical for bone but not lung metastasis. a,b, Bone, lung and liver sections from WT and $Sele^{-/-}$ mice were assessed for E-selectin expression and CD31 co-localization by immunofluorescence. Scale bars, 100 µm. The data are representative of three independent experiments. **c**, BLI quantification of the bone metastasis burden following intracardiac injection of the BM2 cell line into WT or $Sele^{-/-}$ SCID mice. Two-sided Mann–Whitney U tests; $n = 12$ mice per group. **d**, Representative BLI (Day 0 and Day 30), X-ray and µCT images of bone metastases in WT and $Sele^{-/-}$ SCID mice. The images are representative of the median signal from **c**. The white arrows indicate osteolytic lesions. **e**, Quantification of the osteolytic area (right) and the number of osteolytic lesions (left) in the hindlimbs of the animals from **c**. Two-sided Mann–Whitney U tests; $n = 23$ (WT) and 24 ($Sele^{-/-}$) hindlimbs. The data in **c,d,e** are representative of two independent experiments. Data represent the mean ± s.e.m.

Results

Enriched expression of E-selectin in bone specifically promotes bone metastasis. We first tested the correlation between in vitro E-selectin binding and metastatic propensity in vivo. To accurately quantify E-selectin binding across different cell lines, we designed an internally controlled flow cytometry assay (Supplementary Fig. 1a). The fidelity of this assay to detect E-selectin binding was verified using isotype-control IgG, a glycomimetic inhibitor of E-selectin (GMI-1271, uproleselan) and EDTA (Supplementary Fig. 1b). By applying this assay to a panel of isogenic MDA-MB-231 sublines with different organotropic metastatic abilities[25,26], we found that sublines with high bone or lung metastatic abilities generally have increased E-selectin binding ability (Supplementary Fig. 1c,d).

Whereas mouse and xenograft models of colon cancer[27] and melanoma[28] tested in E-selectin knockout ($Sele^{-/-}$) mice[20,29] have demonstrated that E-selectin is not essential for lung metastasis

or primary-tumour formation, the effect of genetic ablation of E-selectin on bone metastasis has not been evaluated. We therefore crossed $Sele^{-/-}$ mice into the non-obese diabetic/severe combined immunodeficiency (NOD/SCID) mouse background for xenograft studies of bone metastasis. Immunofluorescent staining of E-selectin and the endothelial marker CD31 revealed co-localization in the trabecular and cortical bone marrow space in wild-type (WT) mice (Fig. 1a), which is consistent with previous studies[30,31], and E-selectin staining was absent in the bone vasculature of $Sele^{-/-}$ NOD/SCID mice (Fig. 1b). Immunostaining and quantitative PCR (qPCR) demonstrated that E-selectin expression is significantly lower in the lung and liver vasculature compared with bone in both normal (Fig. 1b and Supplementary Fig. 1e) and inflammatory conditions (Supplementary Fig. 1e) known to induce E-selectin expression[30]. Finally, qPCR analysis of pooled RNA collected from human tissues showed a two-fold greater expression

of *CD31*-normalized *Sele* messenger RNA in bones compared with lungs (Supplementary Fig. 1f).

We next analysed bone metastasis of the bone-tropic BM2 (cell line 1833) subline of MDA-MB-231[25] in E-selectin knockout or WT NOD/SCID mice. Bioluminescent imaging (BLI), X-ray and micro–computed tomography (µCT) analyses revealed that genetic knockout of E-selectin significantly attenuated the bone metastatic tumour burden (Fig. 1c–e). A similar result was observed when an in vivo–derived subline of the SUM159 breast cancer line that shows a strong bone metastatic propensity, named SUM159-M1a, was injected into *Sele*^{−/−} mice compared with WT mice (Supplementary Fig. 1g–j). The primary tumour growth of SUM159-M1a was largely unaffected by E-selectin knockout, although an increase in tumour volume in *Sele*^{−/−} mice emerged on the final day of measurement (Supplementary Fig. 1k), which is consistent with a previous report[28].

As the lung metastatic LM2 subline of MDA-MB-231[26] has substantial E-selectin binding ability (Supplementary Fig. 1c), we used this cell line to test the effect of E-selectin knockout on lung metastasis. Knockout of E-selectin did not attenuate lung metastasis; rather, we observed a trend towards increasing total lung metastasis burden in *Sele*^{−/−} NOD/SCID mice (Supplementary Fig. 1l–n). We observed a similar result when the same lung metastasis experiment was performed using SUM159-M1a cells (Supplementary Fig. 1o,p). Together, these data establish that E-selectin is expressed at an elevated level in the bone vasculature and is specifically important for the development of bone metastasis.

Both α1–3 Fut3 and Fut6 promote E-selectin-mediated bone metastasis. Binding of E-selectin to a cell requires the presence of sialyl Lewis X or A (sLe$^{X/A}$) tetrasaccharides at the termini of the cell-surface glycolipids, glycoprotein O-glycans (Ser/Thr-linked) or N-glycans (Asn-linked)[31]. Six fucosyltransferases (Fut3, -4, -5, -6, -7 and -9) are capable of performing the final α1–3 or α1–4 fucosylation to generate sLe$^{X/A}$ (refs. [32–36]). Importantly, Fut4, -7 and -9 are present in both the human and murine genomes, whereas Fut3, -5 and -6 are present only in humans[37]. The contributions of these enzymes to tumorigenesis and organotropic metastasis have not been systematically analysed. Ectopic expression of each Fut in the MDA-MB-231 cell line did not affect the proliferation rates (Supplementary Fig. 2a,b), whereas flow cytometry showed that Fut3, -5, -6 and -7 increase E-selectin binding by several orders of magnitude while Fut4 and Fut9 increase binding by two- to fivefold (Fig. 2a). A similar binding pattern was observed in the SUM159-M1a cell line following the ectopic expression of Fut enzymes (Supplementary Fig. 2c,d).

Intracardiac injection of M1a–Fut cells demonstrated that only the human-specific Fut enzymes (Fut3, -5 and -6) and not Fut7 promoted bone metastasis (Fig. 2b,c and Supplementary Fig. 2e,f), which is supported by previous findings that Fut6 mediates increased engraftment of human mesenchymal stem cells (MSCs) and human prostate cancer cells in bone[38,39]. Clinical analysis of The Cancer Genome Atlas (TCGA) data next revealed that *Fut5* is expressed at low levels in both normal and cancerous human breast tissues compared with more abundant expression of other Fut enzymes (Supplementary Fig. 2g).

To analyse which Fut enzymes endogenously contribute to increased E-selectin binding, the MDA-MB-231 cell line was fluorescence-activated cell sorted into the top and bottom decile of E-selectin binding (Supplementary Fig. 2h). After five passages, E-selectin binding levels were maintained at respectively higher or lower levels (Supplementary Fig. 2i) and qPCR revealed that *Fut3* and *Fut6* expression positively correlated with E-selectin binding, whereas *Fut4* was negatively correlated (Fig. 2d). A similar pattern was observed between different sublines of MDA-MB-231 cells, with elevated *Fut6* and lower *Fut4* expression in a strongly bone metastatic subline (SCP25; Supplementary Fig. 2j).

We next tested whether the bone metastasis-promoting effects of Fut3 and -6 replicated in a spontaneous multi-organ metastasis model. SUM159-M1a cells expressing either of these bone metastasis-promoting Fut enzymes or Fut4 and -7 as negative controls were implanted in the mammary fat pad of NOD/SCID gamma mice. Ectopic Fut3, -4, -6 and -7 expression did not affect primary tumour growth (Fig. 2e), whereas only Fut3 and Fut6 promoted spontaneous bone metastasis and none of the enzymes affected spontaneous lung metastasis (Fig. 2f–h and Supplementary Table 1). To test whether these bone metastasis effects depend on Fut catalytic activity, we generated three catalytic mutants of Fut3 (Fig. 3a). E-selectin binding analysis confirmed that each mutant was catalytically inactive (Fig. 3b). In contrast to the increased bone metastasis caused by overexpression of Fut3, the mutant forms of Fut3 did not promote bone metastasis formation (Fig. 3c–f). In particular, the Y315-stop mutant reduced bone metastasis based on BLI measurements, possibly due to dominant negative effects on WT Fut3 and Fut6.

N-glycoprotein capture mass spectrometry identifies candidate substrates of human Fut enzymes. Given the data showing that increased expression of Fut3 or Fut6 promotes bone metastasis, non-fucosylated glycan substrates of these enzymes must exist in both cell lines (Supplementary Fig. 3a, top). We determined that these are displayed on N-glycans, as M1a and BM2 cells grown with either tunicamycin or 1-deoxymannojirimycin, which block N-linked glycosylation, demonstrated reduced E-selectin binding, whereas D,L-*threo*-PDMP, an inhibitor of glucosylceramide synthase, moderately reduced E-selectin binding to BM2 and did not affect E-selectin binding to M1a cells (Supplementary Fig. 3b,c). Furthermore, GMI-1271, a sLe$^{X/A}$ mimetic, was capable of blocking E-selectin binding to M1a cells expressing each Fut enzyme (Supplementary Fig. 3d), indicating these were conventional E-selectin ligands.

We therefore adapted a solid-phase N-glycoprotein enrichment protocol to comprehensively profile cell surface glycoproteins and identify candidate Fut-enzyme substrates (Supplementary Fig. 3a, bottom)[40,41]. Imaging and flow cytometry controls demonstrated effective ligation of extracellular oxidized glycoproteins (Supplementary Fig. 4a–c). N-glycoproteins were then isolated from MDA-MB-231 and SUM159-M1a cells through: (1) trypsin digestion to remove non-glycosylated peptides, (2) N-glycopeptide release with PNGase F, (3) liquid chromatography–tandem mass spectrometry analysis and (4) computational filtering if peptides that contained one asparagine that was deamidated from PNGase F digestion matched the known N-X-S/T glycosylation motif and were detected in either all four samples or in both samples from a single cell line. Filtering by these criteria resulted in the identification of 1,037 unique N-glycosites that mapped to 541 proteins (Fig. 4a and Supplementary Table 2).

The 361 N-glycosylated proteins shared between the MDA-MB-231 and M1a cells were cross-referenced with reported E-selectin ligands and ranked according to individual N-glycopeptide detection across all four runs by their respective normalized intensities (Supplementary Table 3). The top candidate identified was CD44, which when decorated with sLe^X is known as haematopoietic cell E-/L-selectin ligand (HCELL). HCELL has been attributed as the major E-selectin binding ligand on metastatic cells[23,24,42,43] and HPCs[21]. To determine whether HCELL was responsible for E-selectin binding, we utilized lentiviral clustered regularly interspaced short palindromic repeats (CRISPR)–CRISPR associated protein 9 (Cas9) system to knock out CD44 in the BM2 cell line (Fig. 4b). Loss of CD44 expression did not decrease E-selectin binding in vitro (Fig. 4c) or inhibit bone metastasis in vivo (Supplementary Fig. 4d,e).
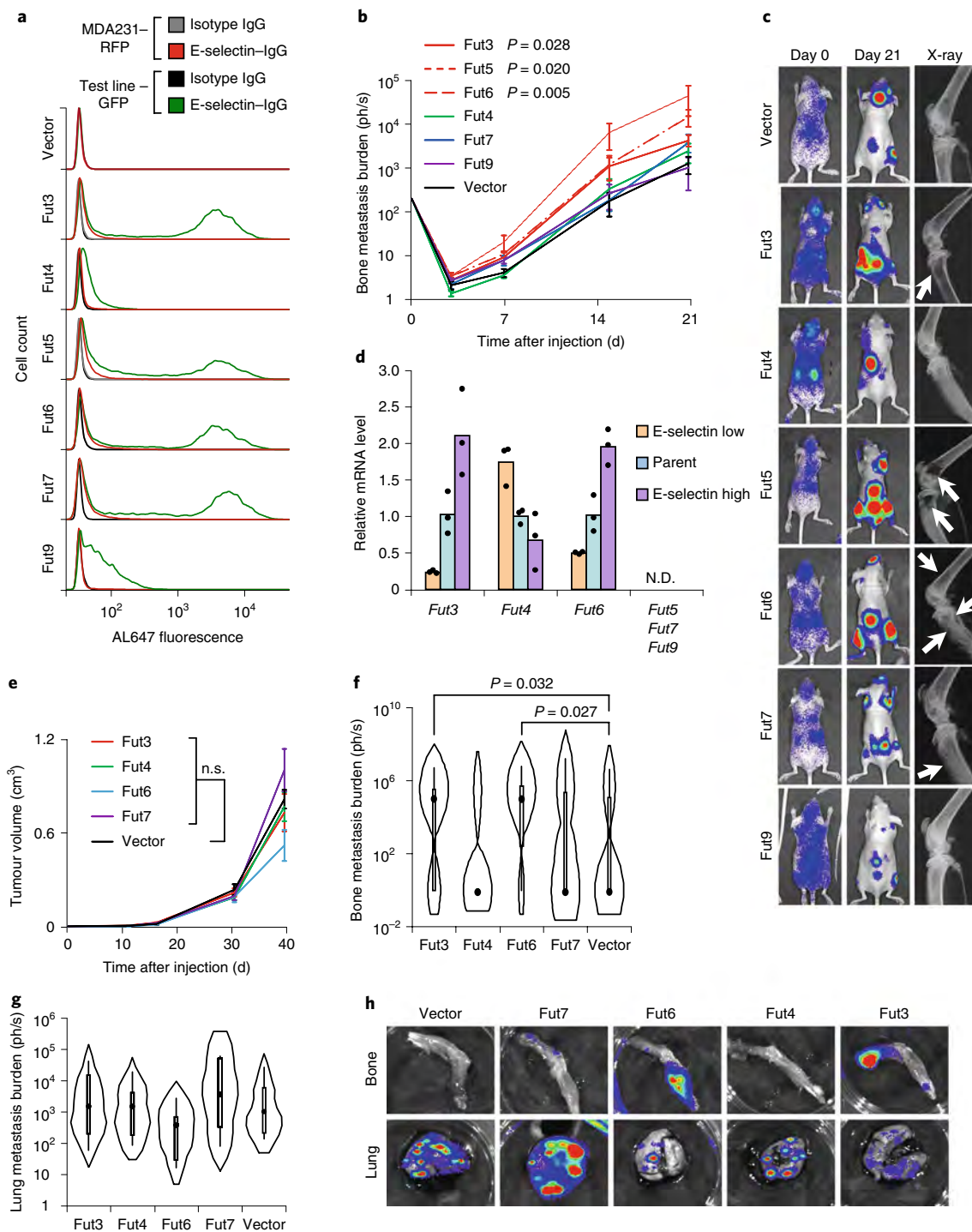
Fig. 2 | Specific α1–3 fucosyltransferases (Fut3 and Fut6) promote bone metastasis. a, Comparative flow cytometry analysis of E-selectin binding to MDA-MB-231 cells with stable ectopic expression of α1–3 Fut enzymes. MDA-MB-231–red fluorescent protein (RFP) was used as an internal control. The data are representative of four independent experiments. **b**, BLI quantification of the bone metastasis burden following intracardiac injection of M1a cells stably expressing each Fut enzyme into Nu/Nu mice. Statistics were performed using two-sided Mann–Whitney U tests at Day 21; $n = 6$ (Fut3, Fut4 and Fut6), 5 (Fut5 and Fut9), 3 (Fut7) and 10 (Vector) mice. **c,** Representative BLI (left and middle) and X-ray (right) images of the bone lesions from **b**. The white arrows indicate osteolytic lesions. **d**, Analysis by qPCR of the endogenous α1–3 Fut mRNA levels in the parental and sorted MDA-MB-231 cells with differential E-selectin binding abilities. Fut5, -7 and -9 were not detectable (N.D.) in any of the cell lines. $n = 3$ technical replicates. **e**, Tumour volume measurements after orthotopic injection of M1a cells stably expressing each relevant Fut enzyme into NOD/SCID gamma mice. Two-sided Student's t-test at Day 39; n.s, not significant; $n = 6$ mice per group. **f,g,** BLI quantification of the spontaneous bone (**f**) and lung (**g**) metastasis burden. The plot elements include the median, box for the interquartile range and spikes to the upper and lower adjacent values. One-sided Mann–Whitney U tests; $n = 11$ lungs and 22 hindlimbs (Fut3 and Fut 4), 6 lungs and 12 hindlimbs (Fut6 and Fut7), and 12 lungs and 24 hindlimbs (Vector). **h**, Representative BLI images of bone and lung tissues from each experimental group. **e–h**, The experiment was performed once. Data represent the mean ± s.e.m. No statistically significant differences ($P > 0.05$) were observed between the Fut4, Fut7 and Fut9 groups versus the Vector group in **b**, the Fut4 and Fut7 groups versus the Vector group in **f**, all group comparisons in **e** and all of the groups versus the Vector group in **g**.
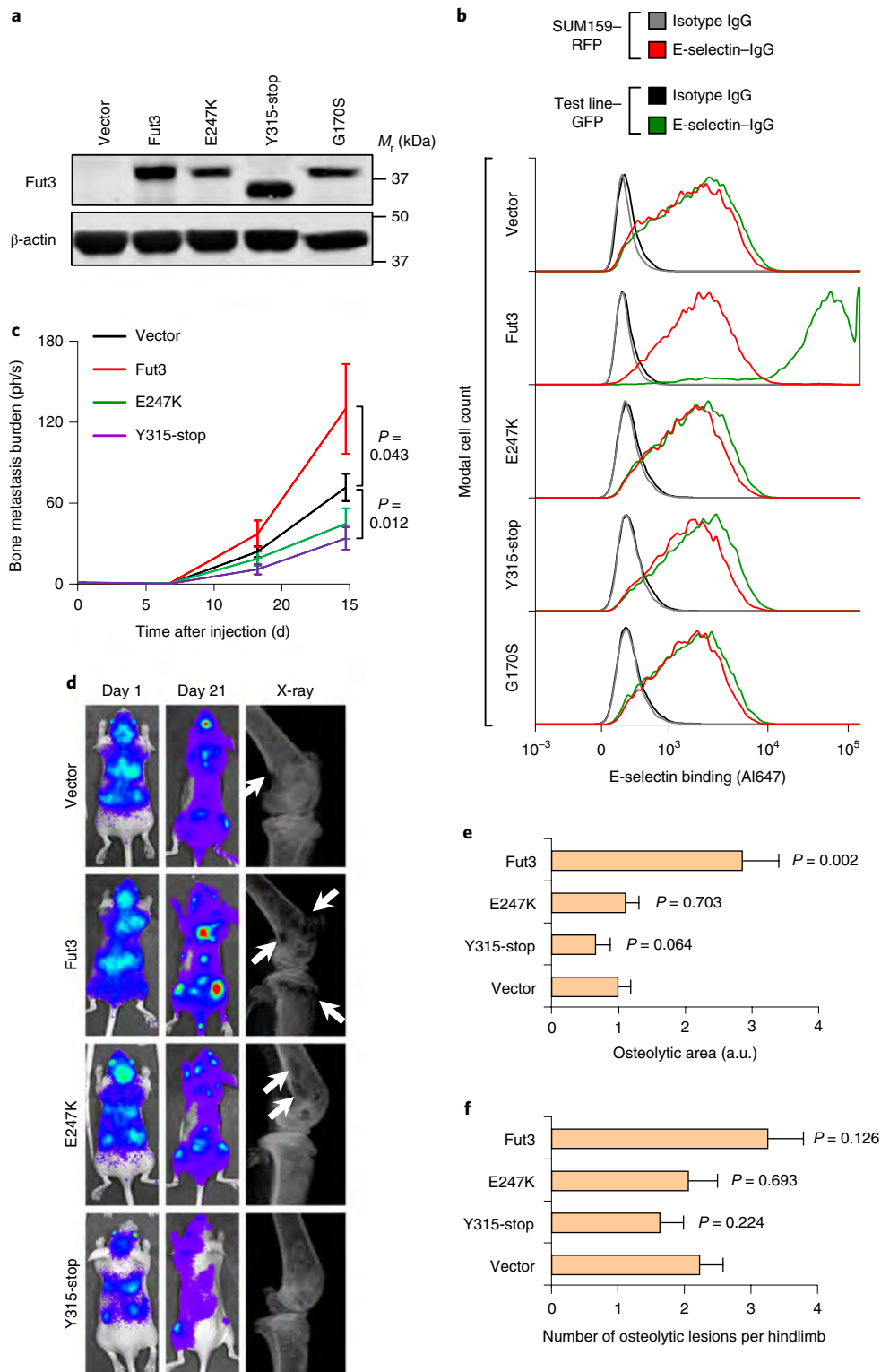
Fig. 3 | In vitro and in vivo characterization of Fut3 catalytic mutants. a, Western blot detection of three Fut3 catalytic mutants compared with WT Fut3 ectopically expressed in SUM159-M1a cells. **b**, Comparative flow cytometry analysis of E-selectin binding to M1a cells expressing each Fut3 mutant using SUM159–RFP as an internal control. The data in **a**,**b** are representative of three independent experiments. **c**, BLI quantification of the bone metastasis burden following intracardiac injection of M1a cells stably expressing each Fut3 mutant compared with vector and WT Fut3. Two-sided Mann–Whitney U tests; $n = 8$ (Fut3 and Y315-stop) and 9 (E247K and Vector) mice per group. **d**, Representative BLI (left and middle) and X-ray (right) images from **c**. **e**,**f**, Quantification of the osteolytic area (**e**) and the number of osteolytic lesions (**f**) in the hindlimbs of Nu/Nu mice receiving an intracardiac injection of M1a cells expressing each Fut3 mutant. Two-sided Mann–Whitney U tests; $n = 16$ (Fut3 and Y315-stop) and 18 (E247K and Vector) hindlimbs per group. **c**–**f**, The experiment was performed once. Data represent the mean ± s.e.m. Unprocessed original scans of the blots in **a** are shown Supplementary Fig. 9.
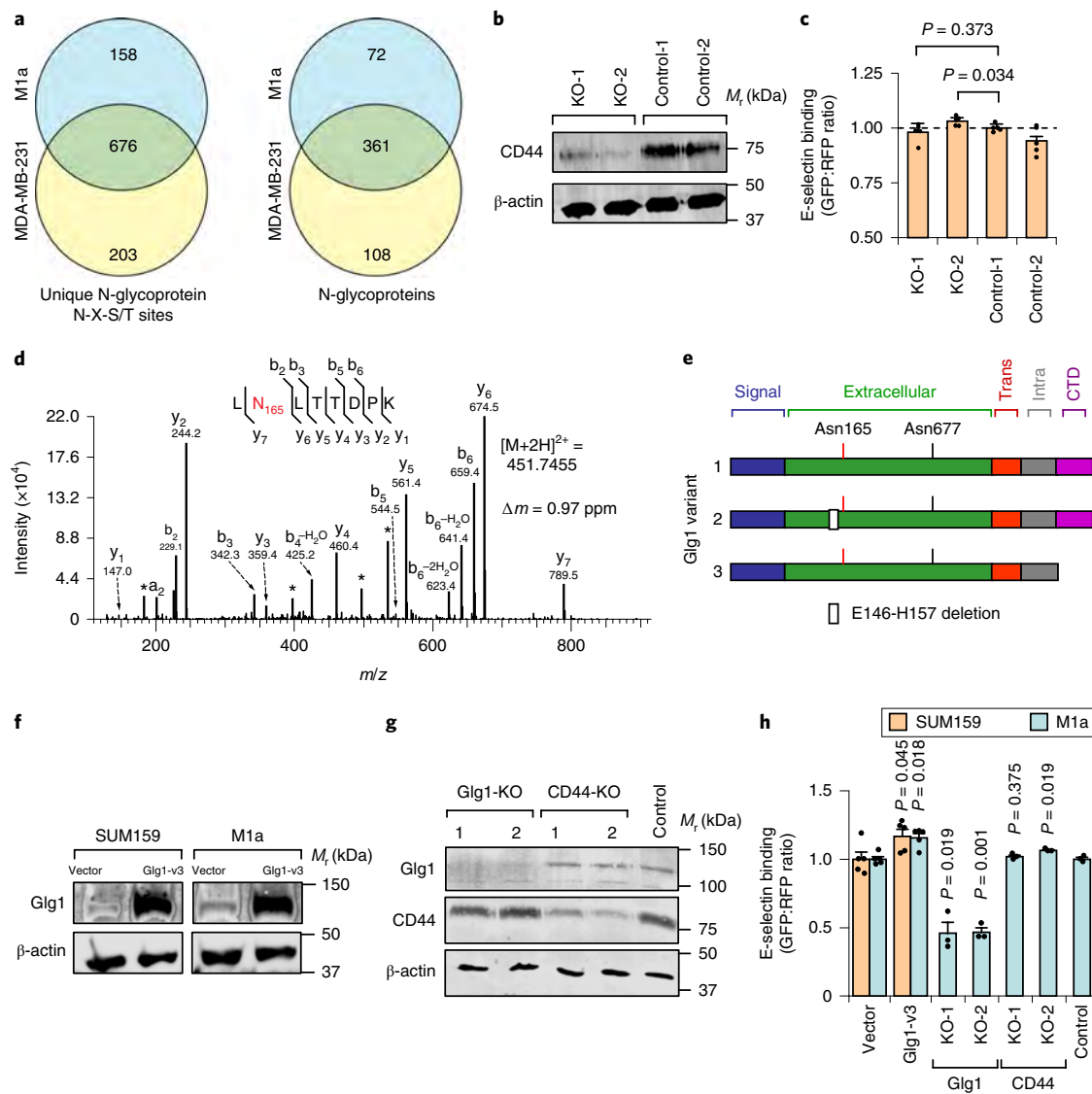
Fig. 4 | Cell surface N-glycan analysis reveals candidate E-selectin ligands in metastatic breast cancer cells. a, Summary of the mass spectrometry results of N-glycosites and N-glycoproteins using two biological replicates of each cell line collected over independent isolations. **b**, Western blot confirming CD44 knockout (KO) by CRISPR–Cas9 in the BM2 cell line. The data are representative of three independent experiments. **c**, Comparative flow cytometry analysis of E-selectin binding to CD44-KO and control BM2 cell lines. MDA-MB-231–RFP was used as an internal control and the binding levels were normalized to Control-1. Two-sided Student's t-tests; $n = 4$ independent biological replicates. **d**, Representative fragmentation spectra of the doubly charged Glg1 tryptic peptide LNLTTDPK containing deamidated Asn(N)165 (red). The N- and C-terminal (b and y) ions matching the predicted peptide fragment are indicated with their respective mass-to-charge (m/z) values. A complete y-ion series was observed, including the site-determining y_7 ion, localizing the deamidation to the Asn residue. The measured doubly charged monoisotopic precursor ion m/z and its mass deviation (Δm) relative to the theoretical m/z are indicated. *, interfering m/z from lower abundance co-isolated ion(s). Similar fragmentation spectra were obtained across independent isolations. **e**, Schematic diagram of the three major Glg1 splice variants in humans. **f**, Western blot analysis of Glg1 expression in SUM159 and M1a cells after stable transduction of retroviral vector expressing Glg1 variant 3 (v3). **g**, Western blot analysis of Glg1 and CD44 after population-level CRISPR–Cas9 knockout of Glg1 and CD44 in M1a cells. The data in **f**,**g** are representative of three independent experiments. **h**, Comparative flow cytometry analysis of E-selectin binding to genetically manipulated SUM159 and M1a cells using SUM159–RFP as an internal control. The binding levels were normalized to respective controls. $n = 5$ (Glg1 and Vector cell lines) and 3 (KO and Control cell lines) independent biological replicates. Two-sided Student's t-tests compare Glg1-v3 cells to Vector cells and CRISPR–Cas9 KO cells to CRISPR–Cas 9 control cells. Data represent the mean ± s.e.m.; CTD, C-terminal domain. Unprocessed original scans of the blots in **b**,**f**,**g** are shown in Supplementary Fig. 9.

Glg1 is functionally important to E-selectin binding of bone metastatic breast cancer cells. N-glycosylation of the second candidate Glg1 (also known as E-selectin ligand 1, Esl1; Fig. 4d,e) was detected at two different residues, with Asn165 detected across all of the samples (Supplementary Table 3). The site and peptide was confirmed by tandem mass spectrometry fragmentation and (as well as) similar elution profiles and extracted ion chromatograms from both cell

lines (Fig. 4d and Supplementary Fig. 4f). Previous research has identified a role for Glg1 in HPCs by maintaining homeostasis or proliferation, possibly in an E-selectin-dependent manner[22,44]. Although Glg1 has been detected in metastatic prostate cells[23,45], the functional importance of Glg1 in cancer has not been investigated.

To test whether *Glg1* expression affected E-selectin binding, isoform-specific primers for the three main Glg1 variants (Fig. 4e)
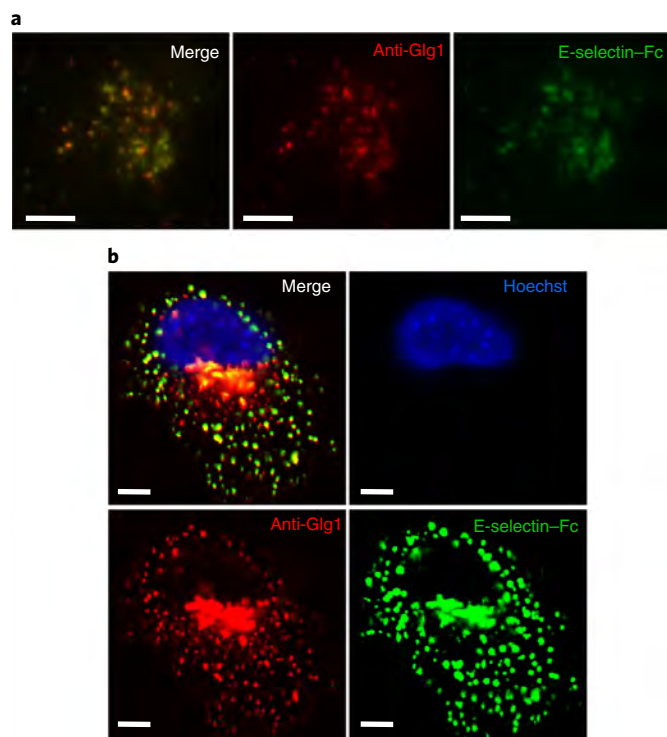
Fig. 5 | E-selectin ligands co-localize with Glg1 at the cell surface.
a, Total internal reflectance fluorescence microscopy at the critical angle using a spinning disc was performed on SUM159-M1a cells probed with recombinant E-selectin–Fc and anti-Glg1. **b**, Confocal *z*-slice of M1a cells probed with E-selectin–Fc, anti-Glg1 and Hoechst. **a,b**, The data are representative of three independent experiments. Scale bars, 5 μm.

were used for qPCR. We found that variants 1 and 3 were enriched in E-selectin high-binding cells (E-high and SCP25), whereas variant 2, which harbours an internal deletion located eight amino acids upstream from the putative Asn165 modification site, was inversely correlated to the E-selectin binding ability (Supplementary Fig. 4g,h). We ectopically expressed Glg1 variants 1 and 3 in SUM159, M1a, MDA-MB-231 and BM2 cells, and knocked out Glg1 in M1a and BM2 cells using lentiviral CRISPR–Cas9 (Fig. 4f,g and Supplementary Fig. 4i–k). The comparative flow cytometry assay revealed that ectopic expression of Glg1 variant 1 and variant 3 increased E-selectin binding to varying degrees in different cell lines, whereas population-level CRISPR–Cas9-mediated knockout of Glg1 reduced E-selectin binding by approximately 50% in the M1a cells and about 20% in the BM2 cell line (Fig. 4h and Supplementary Fig. 4l). Consistent with the result using BM2 cells (Fig. 4c), we observed that CD44 knockout also did not affect E-selectin binding in the M1a cell line (Fig. 4h).

To serve as a bona fide E-selectin ligand, Glg1 must be expressed on the cell membrane and be capable of binding E-selectin. Total internal reflectance fluorescence imaging was performed at the critical angle on M1a cells probed with anti-Glg1 antibody and E-selectin–IgG demonstrated that the Glg1 and E-selectin ligands are displayed on the cell surface, co-localized to the same puncta (Fig. 5a). Furthermore, western blotting of Glg1 revealed its presence in membrane fractions of M1a cells (Supplementary Fig. 5a). Confocal microscopy of permeabilized M1a cells also demonstrated colocalization of Glg1 and E-selectin binding throughout the cell, both at the cell membrane and in internal structures (including the Golgi apparatus and endoplasmic reticulum; Fig. 5b). To assess whether Glg1 directly binds E-selectin, we performed a

western blot under denaturing conditions on cell membrane fractions from M1a Glg1 knockout, Glg1 overexpressing, and Fut3–7 and Fut9 overexpressing cells using E-selectin–IgG as a probe with Fut6-transfected prostate cancer cells (PCR1) serving as a positive control[46]. Although E-selectin–IgG-reactive bands were detectable in the cell membrane fractions of cells expressing Fut3, -5, -6 and -7, E-selectin–IgG-reactive bands were not detected in control, Glg1 knockout, Glg1 overexpression or Fut4 and Fut9 membrane fractions (Supplementary Fig. 5b) despite evidence of E-selectin binding in flow cytometry and immunofluorescence microscopy. Immunoprecipitation of M1a lysates by E-selectin–IgG followed by probing with Glg1 antibody further confirmed that an E-selectin interaction with Glg1 was not detectable using traditional biochemical methods (Supplementary Fig. 5c). Thus, although the data indicate that: (1) N-glycan decoration of proteins but not glycosphingolipids is critical to E-selectin binding, (2) Glg1 is expressed on the cell surface, is N-glycosylated and co-localizes with E-selectin binding, and (3) genetic manipulation of Glg1 leads to significant changes in E-selectin binding levels, we did not obtain evidence that Glg1 directly binds E-selectin.

We next tested whether Glg1 ablation affects metastasis in vivo. Two lentiviral short hairpin RNA (shRNA) constructs targeting all of the *Glg1* splice variants reduced *Glg1*-expression levels in BM2 cells (Supplementary Fig. 6a). Bioluminescent imaging following intracardiac injection confirmed that *Glg1* knockdown reduced the bone metastasis burden (Fig. 6a). Similarly, CRISPR–Cas9-mediated knockout of Glg1 in BM2 and M1a cells resulted in a significant reduction of bone metastasis based on BLI, X-ray and μCT analyses of bone lesions (Fig. 6b–d and Supplementary Fig. 6b–f). In contrast, *Glg1* knockdown in LM2 cells (Supplementary Fig. 6g) did not affect the progression of lung metastasis or survival of the animals (Supplementary Fig. 6h,i). The results were in line with the same observations made with either E-selectin knockout (Fig. 1) or Fut overexpression (Fig. 2).

Pharmaceutical targeting of E-selectin reduces bone metastasis.
Given the identification of E-selectin as a pro-metastatic receptor of the bone vascular niche, the binding of which is predominantly governed by Fut3, Fut6 and Glg1, we sought to assess whether this relationship could predict bone metastasis in human breast cancer. Patients in the NKI-295[47] and EMC-MSK[26,48] datasets were stratified according to the median levels of *Glg1* and *Fut3* or *Fut6* expression and grouped into four cohorts. Those with high expression of both *Glg1* and *Fut3* or *Fut6* suffered from worse prognoses for distant metastasis-free relapse in the NKI-295 datasets (Supplementary Fig. 6j). Organ-specific metastasis data from the EMC-MSK dataset indicated that *Glg1* is a significant prognostic marker of bone metastasis but not of metastasis to the brain, liver or lungs (Supplementary Fig. 6k). Here we analysed data from ER⁻ breast cancer, as metastases in these patients often manifest at multiple organ sites. We further assessed the prognostic potential of each candidate E-selectin ligand identified by mass spectrometry (Supplementary Table 3) in organ-specific metastasis and found the only significant relationship to be that of *Glg1* as a poor prognosis indicator in bone metastasis (Fig. 6e and Supplementary Table 4h).

These results suggest that therapeutic inhibition of E-selectin in patients with tumours expressing a high level of Fut3 or Fut6 and Glg1 may slow down or prevent the progression of bone metastasis. To test this idea, mice were treated twice daily with GMI-1271 at 20 mg kg⁻¹ for 14 d immediately following intracardiac injection with BM2 cells. Bone metastasis-associated bone degradation was attenuated in mice treated with GMI-1271 (Fig. 6f–h). A distinct survival advantage was observed for the mice receiving GMI-1271 (Fig. 6i) and post-mortem μCT bone-volume scans revealed a greater preservation of bone tissue in these mice compared with mice treated with PBS (Fig. 6j).
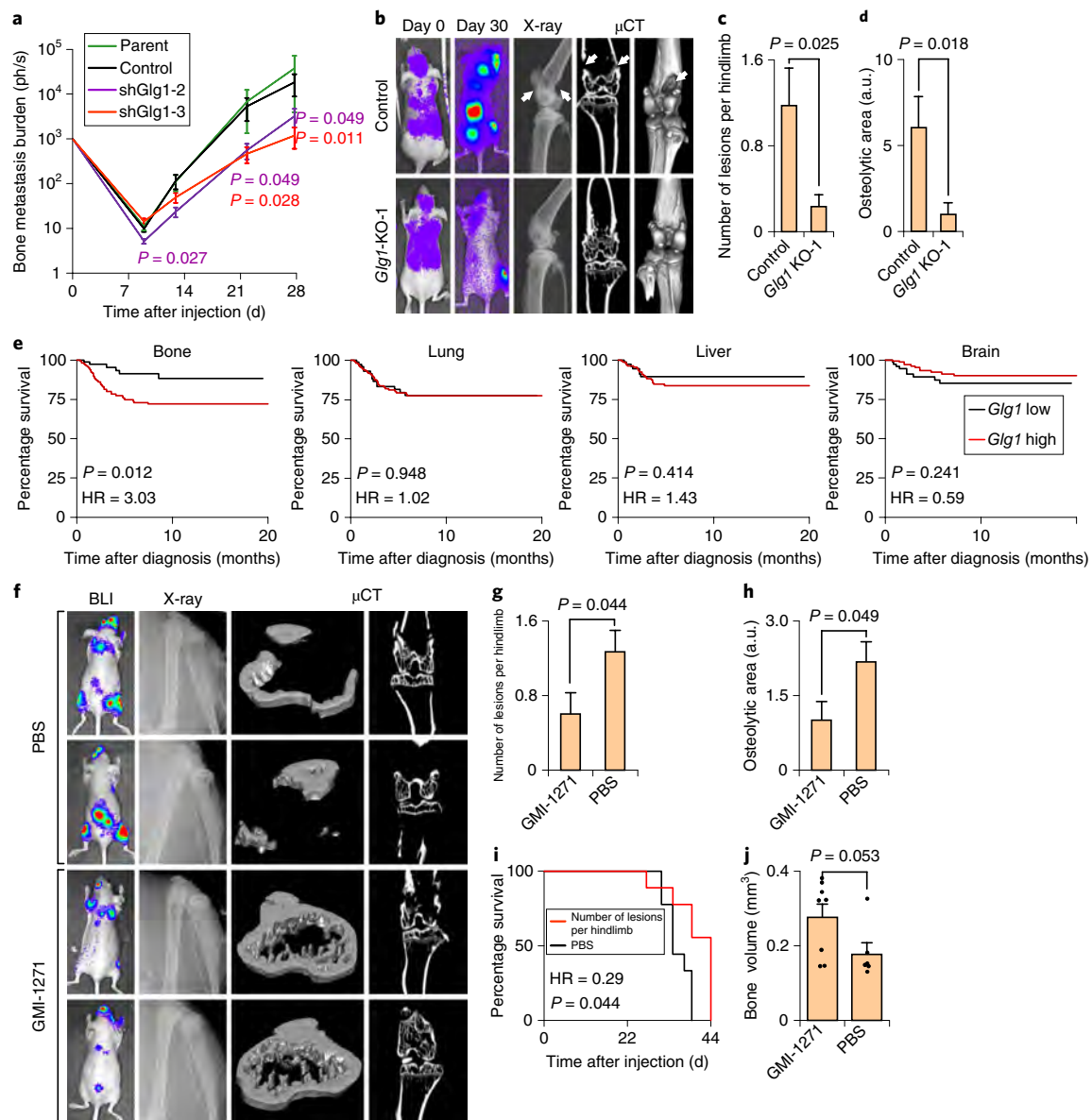
Fig. 6 | Glg1 is required to support bone-metastasis progression. a, BLI quantification of the bone metastasis burden after intracardiac injection of BM2 cells stably expressing *Glg1*-targeting or control shRNA and untransduced (parental) BM2 cells into Nu/Nu mice. Two-sided Mann–Whitney U tests were used to compare the BLI signals of *shGlg1-2* (purple) and *shGlg1-3* (red) with the control; *n* = 8 mice per group. **b**, Representative BLI, X-ray and μCT images from mice injected with BM2 cells modified by CRISPR–Cas9-mediated *Glg1* knockout. The white arrows indicate the osteolytic bone lesions. **c,d**, The number of lesions per hindlimb (**c**) and average osteolytic area (**d**) were quantified from the X-ray images in **b**. Two-sided Mann–Whitney U tests; *n* = 17 hindlimbs per group. The data in **a–d** are representative of two independent experiments. **e**, Kaplan–Meier organ-specific metastasis-free survival curves of ER⁻ breast cancer patients in the EMC-MSK dataset stratified according to the median expression level of *Glg1* mRNA. Two-sided Cox's proportional hazards model; *n* = 244. **f**, Representative BLI, X-ray and μCT images of mice treated with either GMI-1271 or PBS control after intracardiac injection of BM2 cells to generate bone metastasis in Nu/Nu mice. **g,h**, The total number of lesions per hindlimb (**g**) and total osteolytic area (**h**) were quantified between treatments. Two-sided Mann–Whitney U tests; *n* = 12 hindlimbs per group. **i**, Mice from **f** were censored after becoming moribund and followed for Kaplan–Meier survival curve analysis. Two-sided Cox's proportional hazards model; *n* = 9 mice per group. **j**, Bones from moribund mice collected on Day 39 (PBS, *n* = 3) or Day 44 (GMI-1271, *n* = 4) were analysed by μCT and the trabecular bone volume from 4 mm above and below the knee joint was quantified. Two-sided Mann–Whitney U test. **f–j**, The experiment was performed once. Data represent the mean ± s.e.m; HR, hazard ratio.

E-selectin binding promotes a specific MET program. Although the majority of in vitro studies have speculated that E-selectin may promote metastasis by arresting tumour cells in the vasculature of target organs through adhesive interactions[19,27,46], this mechanism is unlikely to be important to bone metastasis as the blood flow in the sinusoidal endothelium of bone marrow has been noted to be particularly slow[49,50] or even stationary[51]. Instead, we considered the possibility that E-selectin engagement of metastatic cells to the endosteal endothelium during the initial phase of bone metastatic colonization (as visualized in Supplementary Fig. 7a) may induce molecular changes in cancer cells that promote bone colonization. This hypothesis was supported by the observation that the growing edge of BM2 bone lesions showed strong Glg1 expression and were associated with a high density of E-selectin⁺ vasculature (Supplementary Fig. 7b).
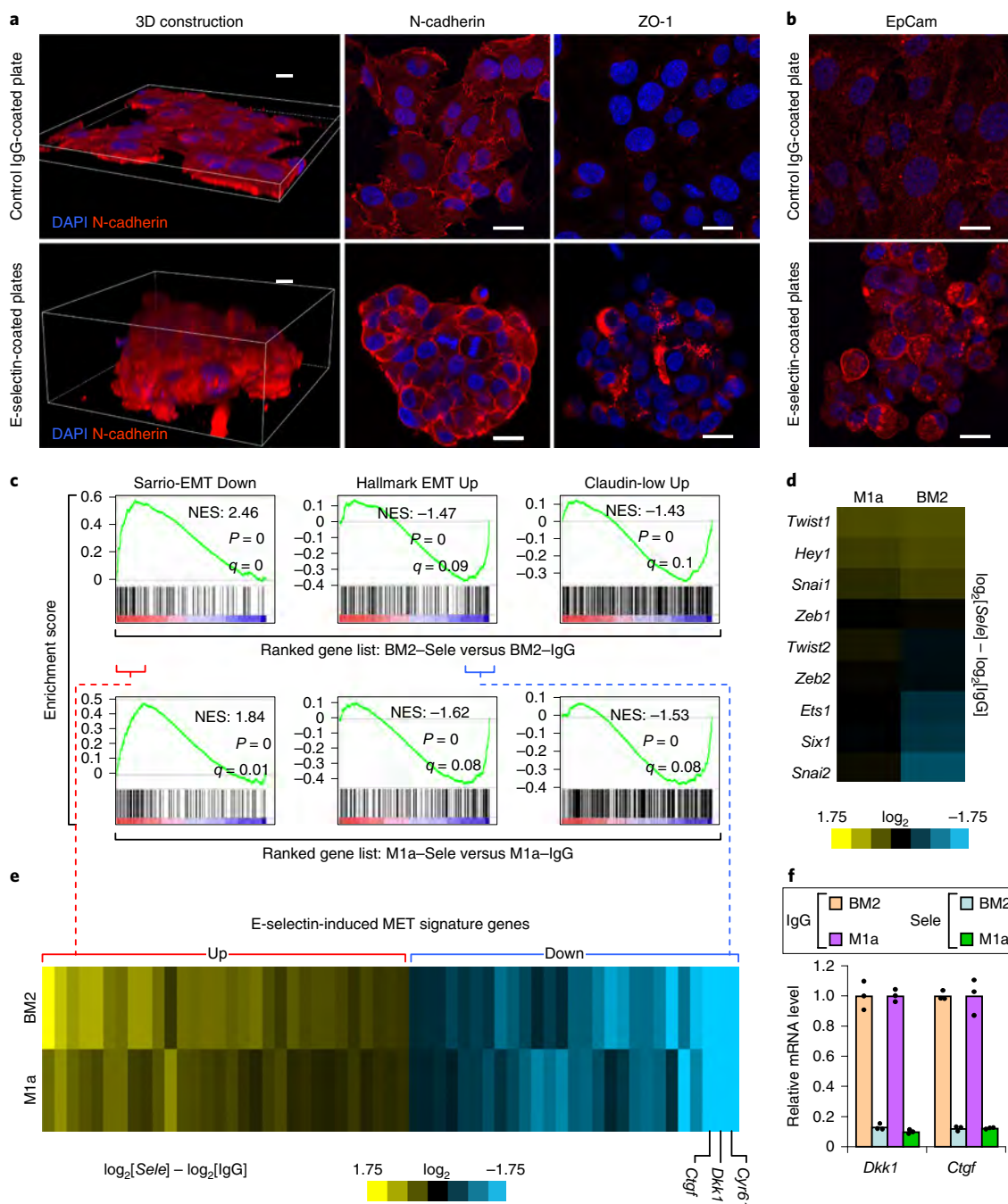
Fig. 7 | E-selectin binding to tumour cells induces a non-canonical MET. a, Confocal imaging of E-selectin-induced morphological changes in M1a cells after culturing on E-selectin- and IgG-coated plates (10 μg ml^{-1}) for 24 h (left). Z-slices of confocal immunofluorescent images demonstrating changes in N-cadherin and ZO-1 localization/expression in M1a cells (right). Scale bars, 10.5 μm (left) and 20 μm (middle and right). **b**, Confocal imaging of EpCam immunofluorescence in BM2 cells seeded over either E-selectin- or IgG-coated plates. Scale bars, 20 μm. The images in **a,b** are representative of three independent experiments. **c**, GSEA of the Sarrio-EMT down (GSE8430), Hallmark EMT up (M5930) and Claudin-low up[61] gene sets in the ranked gene list of the BM2 and M1a cells cultured in E-selectin- versus IgG-coated plates. A single mRNA isolation was used for each condition in each cell line. GSEA software was used to detemine the P and q statistics; n = 108 gene sets queried. **d**, Heat map of the expression of known EMT transcriptional regulators in BM2 and M1a cells cultured in E-selectin- and IgG-coated plates. **e**, Overlapping enrichment-score genes from the Sarrio-EMT down (positive) and Hallmark EMT up (negative) gene sets in the BM2 and M1a cells were compiled to form the E-selectin-induced MET gene signature shown in the heatmap. The gene identities are listed in Supplementary Table 5. **f**, Analysis by qPCR of the *Dkk1* and *Ctgf* mRNA levels in BM2 and M1a cells seeded over IgG or E-selectin for 24 h. n = 3 technical replicates. Data represent the mean ± s.e.m.; NES, normalized enrichment score.

To mimic the engagement of tumour cells to E-selectin, BM2 or M1a cells were seeded on E-selectin- or IgG-coated plates and subjected to spinning-disc microscopy over a period of 40 h. Dramatic differences in cell behaviour and morphology emerged within 3 h of seeding (Supplementary Video 1). Both BM2 and M1a cells migrated along the E-selectin-coated dishes forming three-dimensional clusters ranging in thickness from tens to hundreds of cells, whereas cells that were seeded on IgG plates formed

simple monolayers as in normal tissue culture conditions (Fig. 7a). Immunofluorescence analysis of M1a spheres revealed enriched N-cadherin localization at cell–cell boundaries compared with diffuse staining in cells seeded over IgG. Furthermore, the tight junction protein-1 (TJP-1 or ZO-1) was only detectable in cells seeded on E-selectin (Fig. 7a). Staining for EpCam and Keratin-14 revealed an enhanced shift towards an epithelial state in BM2 spheres (Fig. 7b and Supplementary Fig. 7c).

Microarray and gene set enrichment analysis (GSEA) performed on cells that were seeded for 24 h on either E-selectin- or IgG-coated plates revealed an inverse enrichment of gene signatures related to EMT (Fig. 7c and Supplementary Fig. 7d,e). Unlike traditional models of EMT, E-selectin-induced MET did not affect the RNA expression of the master transcriptional regulators of EMT, such as Snail1/2, Twist1/2 and Zeb1/2 (Fig. 7d). Furthermore, staining of the EMT marker N-cadherin did not show reduced expression but rather altered the localization and apparent molecular weight (Fig. 7a and Supplementary Fig. 7f), whereas protein levels of the Slug transcription factor were much lower after binding E-selectin (Supplementary Fig. 7f). Together, these observations pointed towards a non-canonical MET program that is not the binary opposite of traditional EMT programs. Supporting this, extraction of the enrichment-score genes in the Sarrio-EMT and Hallmark EMT gene sets (Fig. 7c) showed that the majority of the upregulated EMT-associated genes were involved in immune-related processes, whereas the downregulated genes were largely secreted or extracellular proteins (Fig. 7e and Supplementary Table 5). These results indicate that E-selectin binding induces a non-canonical MET-like shift in cancer cells. Finally, staining for epithelial markers revealed ubiquitous E-cadherin and intermittent EpCam staining in BM2 bone lesions (Supplementary Fig. 7g,h), supporting the occurrence of MET during bone metastasis in vivo.

E-selectin-induced MET activates Wnt signalling. The three most downregulated mesenchymal-associated genes (*Dkk1*, *Ctgf* and *Cyr61*) after E-selectin-induced MET encode secreted Wnt repressors[52] (Fig. 7e,f). We next investigated whether repression of these Wnt inhibitors by E-selectin-induced MET could activate Wnt signalling, as Wnt signalling has been reported to promote cancer stem cell activities during metastasis[53]. To this end, we introduced a 7×TCF–GFP Wnt reporter plasmid[54] into BM2 cells (BM2-TGC). Cells seeded on E-selectin for 48 h activated this Wnt reporter to levels similar to cells seeded on IgG and treated with recombinant Wnt3a (Fig. 8a). Live imaging revealed that MET occurred in the first several hours, whereas Wnt activation occurred 30 h after binding (Supplementary Video 1). Quantitative PCR revealed that multiple Wnt target genes, including those related to cancer stem cells (for example, *Sox2* and *Sox9*) were induced by plating tumour cells on E-selectin, whereas the canonical EMT markers *Vim*, *Zeb1* and *Zeb2* remained mostly unchanged (Fig. 8b), consistent with results from gene expression profiling analysis (Fig. 7d), thus confirming that E-selectin activated canonical Wnt signalling. Ex vivo microscopy of BM2-TGC bone lesions demonstrated that Wnt signalling was active in cells that were in a high density of CD31^{+} vasculature (Fig. 8c and Supplementary Fig. 8a).

Ectopic expression of Dkk1–FLAG in BM2-TGC cells (Supplementary Fig. 8b) blocked Wnt activation following exposure to Wnt3a-conditioned media but exerted a lesser effect on E-selectin-mediated Wnt signalling. In contrast, inhibitors of β-catenin-TCF binding (ICG-001 and LF3) disrupted E-selectin-mediated Wnt signalling while exerting less of an effect on paracrine-mediated Wnt activation (Supplementary Fig. 8c). Treatment of BM2 bone metastases with LF3 did not exhibit observable toxicity but reduced the number of osteolytic lesions (Supplementary Fig. 8d–f).

Recent glycomic analysis has found a strong correlation between extracellular fucosylation and epithelial features[55]. Quantitative PCR analysis of the levels of *Glg1-variant 3*, *Fut3* and *Fut6* 48 h after seeding on E-selectin confirmed that E-selectin-induced MET led to increased expression of the genes responsible for the binding of tumour cells to E-selectin (Fig. 8d), indicating the existence of a positive feedback loop. This finding is consistent with the stronger Glg1 staining in metastatic cancer cells in close contact with the bone vasculature (Supplementary Fig. 7b). To investigate whether this Wnt activation contributed to cancer stem cell identity, we transduced BM2 cells with a Sox2/Oct4–mCherry (SORE6–mCherry) cancer stem cell reporter[53]. When plated on IgG, 11% of these cells were positive for Sox2/Oct4 but this increased to 31.7% after binding to E-selectin-coated plates, indicating an increase in cancer stemness activity following binding to E-selectin (Fig. 8e).

Finally, we wanted to understand whether this mechanism extended to other models of bone metastasis and whether the discovered mechanism is relevant to clinical bone metastasis patients. We therefore used in vivo selection to derive a bone metastatic subline (named ob1) from the DU145 prostate cancer cell line[56]. Flow cytometry revealed this subline binds E-selectin (Supplementary Fig. 8g). Similar to breast cancer studies, E-selectin knockout mice exhibited lower bone metastasis colonization and survived longer than WT hosts following intracardiac injection of DU145-ob1 (Supplementary Fig. 8h,i). Plating of these cells on E-selectin-coated plates revealed a similar phenomenon of clustering and a shift towards epithelial features (Supplementary Fig. 8j). Furthermore, immunostaining of E-selectin, Glg1 and Ki67 in bone metastasis biopsies from prostate cancer patients demonstrated an association between E-selectin expression and Glg1^{+} tumour cells that are proliferative (Ki67^{+}; Supplementary Fig. 8k).

Discussion

Although numerous studies have established that EMT is often necessary for the escape from a primary tumour[7] and others have shown that these cells must revert to an epithelial state to successfully colonize an organ[11–13], the lack of evidence for how MET is induced, especially in the context-dependent manner required for metastatic colonization in a distant organ, has resulted in considerable controversy within the field. Here we provide evidence that a unique stromal cue—binding to E-selectin via Fut3/6 and Glg1 expressed by bone metastatic cells—induces MET to facilitate bone metastasis. The data further indicate that this non-canonical MET activates Wnt signalling to promote stemness via Sox2/9 expression and further increases Glg1 and Fut3/6 expression (Fig. 8f).

E-selectin-induced MET is a non-canonical program compared with MET inducers such as miR-200 that target the master transcription factors of EMT[57]. Rather, a key function of E-selectin-induced MET is the activation of Wnt signalling, a pathway linked to self-renewal, cancer stem cell traits and EMT induction[58]. This reported link between Wnt-induced stemness and EMT is incompatible with the requirement for MET during metastatic colonization, which therefore raises an interesting paradox: how can MET and cancer stemness coexist during metastatic colonization? By linking E-selectin-induced MET with Wnt signalling and *Sox2/9* induction, we show how E-selectin engagement could resolve this paradox in bone metastasis, which is akin to recent findings showing that Prrx1 uncouples EMT from stemness traits during lung metastasis[11].

Our discovery of the crucial role of E-selectin in bone metastasis raises the question of why no previous studies have shown a functional effect of E-selectin. Three discoveries made here explain a possible cause: (1) Fut3/6 are responsible for generating functional E-selectin ligands, thus implying that murine models of bone metastasis may not be dependent on E-selectin, (2) E-selectin-induced Wnt activation occurred 30 h after binding, whereas previous in vivo studies of E-selectin were performed within 6 h of injection[42,59] and (3) the organ-specific expression pattern of E-selectin indicates
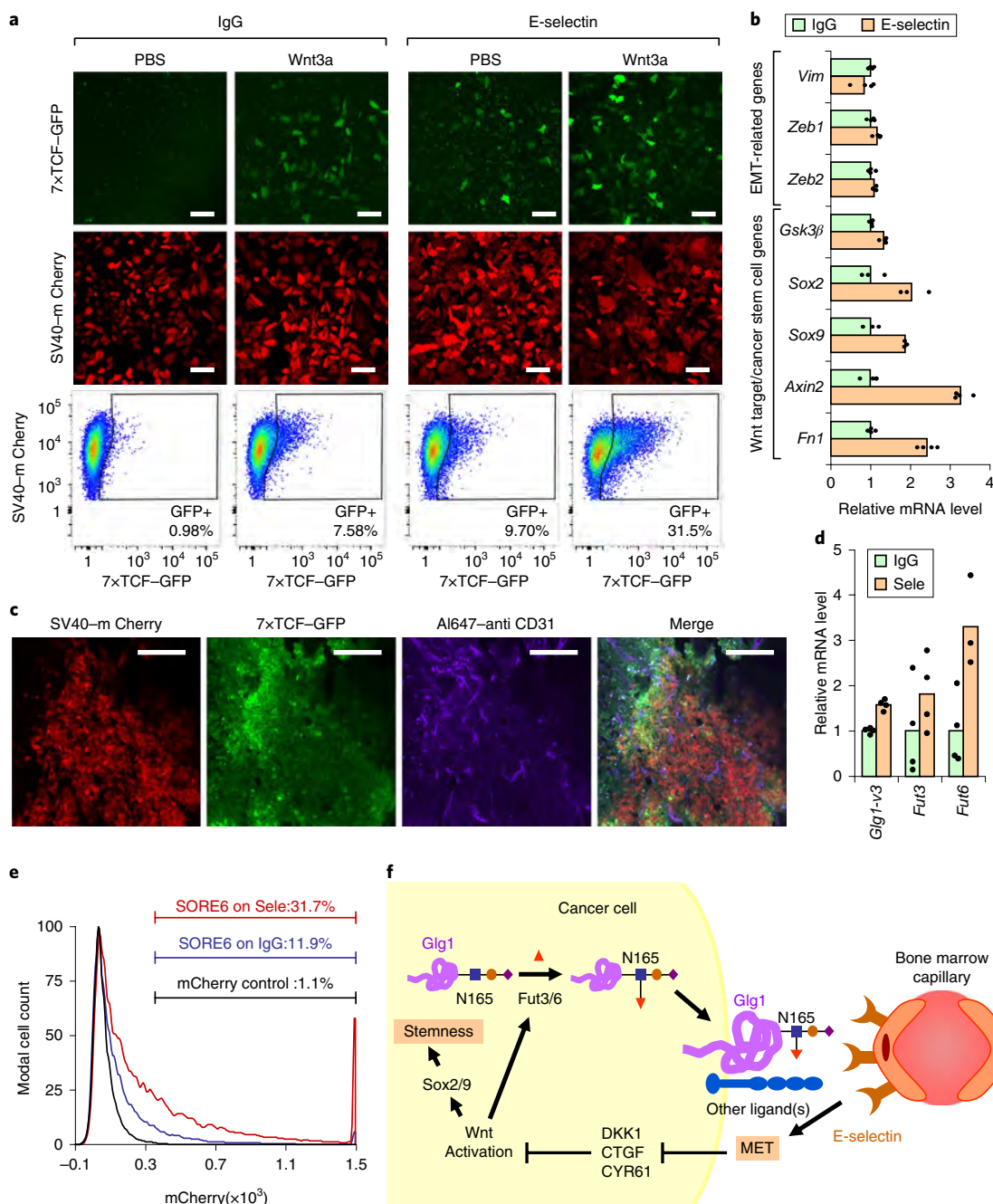
Fig. 8 | E-selectin-induced MET activates Wnt signalling. a, BM2 cells stably expressing the 7×TCF–GFP reporter and SV40–mCherry as an internal control (BM2-TGC) were plated on either E-selectin or IgG-coated (10 μg ml^{-1}) plates with or without recombinant Wnt3a (100 ng ml^{-1}). Fluorescence was assessed by confocal microscopy after 48 h (top) and quantified by flow cytometry (bottom). Scale bars, 100 μm. The data are representative of at least five independent experiments. **b**, Analysis by qPCR of EMT- and Wnt-associated genes from the BM2 cells plated on E-selectin or IgG (10 μg ml^{-1}) for 48 h. $n = 3$ technical replicates. **c**, Ex vivo confocal images of bone metastasis in Nu/Nu mice injected with BM2-TGC. Live animal labelling with anti-CD31 was conducted to visualize the vasculature. Scale bars, 100 μm. The data are representative of four biological replicates. **d**, Analysis by qPCR of the levels of *Glg1-variant 3* (*v3*), *Fut3* and *Fut6* in BM2 cells seeded on either IgG or E-selectin (10 μg ml^{-1}) for 48 h. $n = 4$ technical replicates. **e**, BM2 cells stably expressing the SORE6–mCherry stemness reporter or control mCherry reporter were plated on E-selectin or control IgG (10 μg ml^{-1}) for 48 h. The fluorescence of mCherry was assessed by flow cytometry after 48 h. The data are representative of three independent biological replicates. **f**, Proposed model of E-selectin function during bone metastasis.

it is most relevant to bone metastasis as compared with lung or liver metastasis[27]. Interestingly, in a transgenic mouse model of E-selectin under the control of the β-actin promoter, the murine B16F10 cell line could be redirected to the liver only if both *Fut3* and E-selectin were ectopically expressed in the cell line and liver endothelium[60].

Our discovery that Glg1 is instrumental to MET during bone metastasis and co-localizes with E-selectin ligands opens numerous avenues for further research to elucidate whether it chaperones ligand maturation or expression, and how it may function as an intermediate between E-selectin binding and MET induction. The common dependence of MDA-MB-231, SUM159 breast cancer

cells and DU145 prostate cancer cells on E-selectin binding to achieve bone metastasis, together with the prognostic significance of Glg1 and Fut3/Fut6 in clinical bone metastasis, indicate that the discovered pathway is probably a conserved mechanism that facilitates tumour–endothelial interaction during metastatic seeding in bone. Therapeutic agents targeting the E-selectin ligand-mediated pathway, such as LF3 or GMI-1271, may be developed for the treatment of bone metastasis.

Online content

Any methods, additional references, Nature Research reporting summaries, source data, statements of data availability and associated accession codes are available at https://doi.org/10.1038/s41556-019-0309-2.

References

1. Valastyan, S. & Weinberg, R. A. Tumor metastasis: molecular insights and evolving paradigms. *Cell* **147**, 275–292 (2011).
2. Massagué, J. & Obenauf, A. C. Metastatic colonization by circulating tumour cells. *Nature* **529**, 298–306 (2016).
3. Yang, J. & Weinberg, R. A. Epithelial-mesenchymal transition: at the crossroads of development and tumor metastasis. *Dev. Cell* **14**, 818–829 (2008).
4. Nieto, M. A., Huang, R. Y., Jackson, R. A. & Thiery, J. P. EMT: 2016. *Cell* **166**, 21–45 (2016).
5. Esposito, M., Guise, T. & Kang, Y. The biology of bone metastasis. *Cold Spring Harb. Perspect. Med.* **8**, a031252 (2018).
6. Oskarsson, T., Batlle, E. & Massagué, J. Metastatic stem cells: sources, niches, and vital pathways. *Cell Stem Cell* **14**, 306–321 (2014).
7. Yang, J. et al. Twist, a master regulator of morphogenesis, plays an essential role in tumor metastasis. *Cell* **117**, 927–939 (2004).
8. Mani, S. A. et al. The epithelial-mesenchymal transition generates cells with properties of stem cells. *Cell* **133**, 704–715 (2008).
9. Labelle, M., Begum, S. & Hynes, R. O. Direct signaling between platelets and cancer cells induces an epithelial-mesenchymal-like transition and promotes metastasis. *Cancer Cell* **20**, 576–590 (2011).
10. Brabletz, T. et al. Variable β-catenin expression in colorectal cancers indicates tumor progression driven by the tumor environment. *Proc. Natl Acad. Sci. USA* **98**, 10356–10361 (2001).
11. Ocana, O. H. et al. Metastatic colonization requires the repression of the epithelial-mesenchymal transition inducer Prrx1. *Cancer Cell* **22**, 709–724 (2012).
12. Tsai, J. H., Donaher, J. L., Murphy, D. A., Chau, S. & Yang, J. Spatiotemporal regulation of epithelial-mesenchymal transition is essential for squamous cell carcinoma metastasis. *Cancer Cell* **22**, 725–736 (2012).
13. Korpal, M. et al. Direct targeting of Sec23a by miR-200s influences cancer cell secretome and promotes metastatic colonization. *Nat. Med.* **17**, 1101–1108 (2011).
14. Celià-Terrassa, T. et al. Epithelial-mesenchymal transition can suppress major attributes of human epithelial tumor-initiating cells. *J. Clin. Invest.* **122**, 1849–1868 (2012).
15. Liu, Y. et al. Mouse fibroblasts lacking RB1 function form spheres and undergo reprogramming to a cancer stem cell phenotype. *Cell Stem Cell* **4**, 336–347 (2009).
16. Chiou, S. H. et al. Coexpression of Oct4 and Nanog enhances malignancy in lung adenocarcinoma by inducing cancer stem cell-like properties and epithelial-mesenchymal transdifferentiation. *Cancer Res.* **70**, 10433–10444 (2010).
17. Shiozawa, Y. et al. Human prostate cancer metastases target the hematopoietic stem cell niche to establish footholds in mouse bone marrow. *J. Clin. Invest.* **121**, 1298–1312 (2011).
18. Ghajar, C. M. et al. The perivascular niche regulates breast tumour dormancy. *Nat. Cell Biol.* **15**, 807–817 (2013).
19. Walz, G., Aruffo, A., Kolanus, W., Bevilacqua, M. & Seed, B. Recognition by ELAM-1 of the sialyl-Lex determinant on myeloid and tumor cells. *Science* **250**, 1132–1135 (1990).
20. Frenette, P. S., Mayadas, T. N., Rayburn, H., Hynes, R. O. & Wagner, D. D. Double knockout highlights value of endothelial selectins. *Immunol. Today* **17**, 205 (1996).
21. Dimitroff, C. J., Lee, J. Y., Rafii, S., Fuhlbrigge, R. C. & Sackstein, R. CD44 is a major E-selectin ligand on human hematopoietic progenitor cells. *J. Cell Biol.* **153**, 1277–1286 (2001).

22. Winkler, I. G. et al. Vascular niche E-selectin regulates hematopoietic stem cell dormancy, self renewal and chemoresistance. *Nat. Med.* **18**, 1651–1657 (2012).
23. Dimitroff, C. J. et al. Identification of leukocyte E-selectin ligands, P-selectin glycoprotein ligand-1 and E-selectin ligand-1, on human metastatic prostate tumor cells. *Cancer Res.* **65**, 5750–5760 (2005).
24. Hanley, W. D., Burdick, M. M., Konstantopoulos, K. & Sackstein, R. CD44 on LS174T colon carcinoma cells possesses E-selectin ligand activity. *Cancer Res.* **65**, 5812–5817 (2005).
25. Kang, Y. et al. A multigenic program mediating breast cancer metastasis to bone. *Cancer Cell* **3**, 537–549 (2003).
26. Minn, A. J. et al. Genes that mediate breast cancer metastasis to lung. *Nature* **436**, 518–524 (2005).
27. Läubli, H. & Borsig, L. Selectins as mediators of lung metastasis. *Cancer Microenviron.* **3**, 97–105 (2010).
28. Taverna, D. et al. Increased primary tumor growth in mice null for β3- or β3/β5-integrins or selectins. *Proc. Natl Acad. Sci. USA* **101**, 763–768 (2004).
29. Labow, M. A. et al. Characterization of E-selectin-deficient mice: demonstration of overlapping function of the endothelial selectins. *Immunity* **1**, 709–720 (1994).
30. Khatib, A. M. et al. Rapid induction of cytokine and E-selectin expression in the liver in response to metastatic tumor cells. *Cancer Res.* **59**, 1356–1361 (1999).
31. Lowe, J. B. Glycan-dependent leukocyte adhesion and recruitment in inflammation. *Curr. Opin. Cell Biol.* **15**, 531–538 (2003).
32. Mondal, N. et al. Distinct human α(1,3)-fucosyltransferases drive Lewis-X/sialyl Lewis-X assembly in human cells. *J. Biol. Chem.* **293**, 7300–7314 (2018).
33. Mollicone, R. et al. Molecular basis for Lewis α(1,3/1,4)-fucosyltransferase gene deficiency (FUT3) found in Lewis-negative Indonesian pedigrees. *J. Biol. Chem.* **269**, 20987–20994 (1994).
34. Oulmouden, A. et al. Molecular cloning and expression of a bovine α(1,3)-fucosyltransferase gene homologous to a putative ancestor gene of the human FUT3-FUT5-FUT6 cluster. *J. Biol. Chem.* **272**, 8764–8773 (1997).
35. Goelz, S. E. et al. ELFT: a gene that directs the expression of an ELAM-1 ligand. *Cell* **63**, 1349–1356 (1990).
36. Buffone, A. et al. Silencing α1,3-fucosyltransferases in human leukocytes reveals a role for FUT9 enzyme during E-selectin-mediated cell adhesion. *J. Biol. Chem.* **288**, 1620–1633 (2013).
37. Costache, M. et al. Evolution of fucosyltransferase genes in vertebrates. *J. Biol. Chem.* **272**, 29721–29728 (1997).
38. Li, J. et al. Human fucosyltransferase 6 enables prostate cancer metastasis to bone. *Br. J. Cancer* **109**, 3014–3022 (2013).
39. Sackstein, R. et al. Ex vivo glycan engineering of CD44 programs human multipotent mesenchymal stromal cell trafficking to bone. *Nat. Med.* **14**, 181–187 (2008).
40. Ossola, R. et al. Biomarker validation in blood specimens by selected reaction monitoring mass spectrometry of N-glycosites. *Methods Mol. Biol.* **728**, 179–194 (2011).
41. Weekes, M. P. et al. Proteomic plasma membrane profiling reveals an essential role for gp96 in the cell surface expression of LDLR family members, including the LDL receptor and LRP6. *J. Proteome Res.* **11**, 1475–1484 (2012).
42. Price, T. T. et al. Dormant breast cancer micrometastases reside in specific bone marrow niches that regulate their transit to and from bone. *Sci. Transl. Med.* **8**, 340ra373 (2016).
43. Morita, Y. et al. E-selectin targeting PEGylated-thioaptamer prevents breast cancer metastases. *Mol. Ther. Nucleic Acids* **5**, e399 (2016).
44. Sreeramkumar, V. et al. Coordinated and unique functions of the E-selectin ligand ESL-1 during inflammatory and hematopoietic recruitment in mice. *Blood* **122**, 3993–4001 (2013).
45. Yasmin-Karim, S., King, M. R., Messing, E. M. & Lee, Y. F. E-selectin ligand-1 controls circulating prostate cancer cell rolling/adhesion and metastasis. *Oncotarget* **5**, 12097–12110 (2014).
46. Barthel, S. R. et al. Definition of molecular determinants of prostate cancer cell bone extravasation. *Cancer Res.* **73**, 942–952 (2013).
47. van de Vijver, M. J. et al. A gene-expression signature as a predictor of survival in breast cancer. *N. Engl. J. Med.* **347**, 1999–2009 (2002).
48. Wang, Y. et al. Gene-expression profiles to predict distant metastasis of lymph-node-negative primary breast cancer. *Lancet* **365**, 671–679 (2005).
49. Winkler, I. G. et al. Positioning of bone marrow hematopoietic and stromal cells relative to blood flow in vivo: serially reconstituting hematopoietic stem cells reside in distinct nonperfused niches. *Blood* **116**, 375–385 (2010).
50. Pries, A. R. & Kuebler, W. M. in *Handbook of Experimental Pharmacology*, Vol. 176/I (eds Moncada, S. & Higgs, A.) 1–40 (Springer, 2006).
51. Bixel, M. G. et al. Flow dynamics and HSPC homing in bone marrow microvessels. *Cell Rep.* **18**, 1804–1816 (2017).
52. Macdonald, B. T., Semenov, M. V. & He, X. SnapShot: Wnt/β-catenin signaling. *Cell* **131**, 1204 (2007).
53. Tang, B. et al. A flexible reporter system for direct observation and isolation of cancer stem cells. *Stem Cell Rep.* **4**, 155–169 (2015).

54. Fuerer, C. & Nusse, R. Lentiviral vectors to probe and manipulate the Wnt signaling pathway. *PLoS One* **5**, e9370 (2010).
55. Holst, S. et al. N-glycosylation profiling of colorectal cancer cell lines reveals association of fucosylation with differentiation and caudal type homebox 1 (CDX1)/Villin mRNA expression. *Mol. Cell. Proteomics* **15**, 124–140 (2016).
56. Stone, K. R., Mickey, D. D., Wunderli, H., Mickey, G. H. & Paulson, D. F. Isolation of a human prostate carcinoma cell line (DU 145). *Int J. Cancer* **21**, 274–281 (1978).
57. Korpal, M., Lee, E. S., Hu, G. & Kang, Y. The miR-200 family inhibits epithelial-mesenchymal transition and cancer cell migration by direct targeting of E-cadherin transcriptional repressors ZEB1 and ZEB2. *J. Biol. Chem.* **283**, 14910–14914 (2008).
58. Anastas, J. N. & Moon, R. T. WNT signalling pathways as therapeutic targets in cancer. *Nat. Rev. Cancer* **13**, 11–26 (2013).
59. Sipkins, D. A. et al. In vivo imaging of specialized bone marrow endothelial microdomains for tumour engraftment. *Nature* **435**, 969–973 (2005).
60. Biancone, L., Araki, M., Araki, K., Vassalli, P. & Stamenkovic, I. Redirection of tumor metastasis by expression of E-selectin in vivo. *J. Exp. Med.* **183**, 581–587 (1996).
61. Herschkowitz, J. I. et al. Identification of conserved gene expression features between murine mammary carcinoma models and human breast tumors. *Genome Biol.* **8**, R76 (2007).

Author contributions

M.E. and Y.K. conceived the project and co-wrote the manuscript. M.E. designed and conducted all of the flow cytometry, xenograft, genetic, qRT–PCR, confocal and bioinformatic experiments, and analysed the data. M.E. derived the SUM159-M1a and DU145-ob1 cell lines. T.M.G., M.E. and I.M.C. performed the mass spectrometry and analysed the data. N.M. and R.S. performed the E-selectin immunoprecipitation experiments, provided advice and assisted in writing the manuscript. Y.W., C.S., H.Z. and C.C. assisted with the mouse experiments and stable cell generation. Y.W. and M.E. performed and analysed the microarray experiments. S.-C.L. and S.-H.L. stained the prostate-cancer bone biopsies. J.L.M. provided GMI-1271 and research input.

Additional information

Supplementary information is available for this paper at https://doi.org/10.1038/s41556-019-0309-2.

Reprints and permissions information is available at www.nature.com/reprints.

Correspondence and requests for materials should be addressed to Y.K.

Methods

Cell lines, cell culture and human prostate cancer specimens. MDA-MB-231 cells and its derivatives[25,26], and DU145 cells[56] and its derivatives were cultured in DMEM and RPMI media, respectively, supplemented with 10% fetal bovine serum (FBS) and pen/strep. The SUM159 cell line[62], its highly metastatic M1a subline and all of the derivative sublines were grown in F12 media supplemented with 10% FBS, 10 µg ml^{−1} insulin and 20 ng ml^{−1} epidermal growth factor. The M1a cell line was derived from sequential in vivo selection, first from a SUM159 primary tumour, which was dissociated and cultured, and then from a lung metastatic node following tail-vein injection of this culture. Both selections were performed in athymic Nu/Nu female mice. The ob1 cell line was derived from an osteoblastic lesion in Nu/Nu mice injected with DU145-GFP, expanded in culture and validated to have increased bone metastatic ability in vivo. Cell lines were labelled with retroviral vectors with bi-cistronic expression of GFP/firefly luciferase or RFP/renilla luciferase to facilitate the imaging and flow cytometry experiments. The PCR1 cell line that was used to prepare cell lysates was a gift from S. Barthel[46]. All of the cell lines were verified to be negative for mycoplasma contamination by monthly PCR analysis. No of the cells lines used here appear in the database of commonly misidentified cell lines (ICLAC). All of the cell lines were validated with STR analysis and compared with NCBI repository data. The major characteristics of key cell lines used in the study are listed in Supplementary Table 6.

Human prostate cancer bone metastasis specimens were archived, anonymized specimens obtained from the MDACC prostate cancer tissue bank through a protocol approved by the MD Anderson Cancer Center Institutional Review Board. The study is compliant with all of the relevant ethical regulations regarding research involving human participants and informed consent was obtained from all participants.

Mouse models and xenografts. All procedures involving mice and experimental protocols were approved by the University Institutional Animal Care and Use Committee (IACUC). The study is compliant with all relevant ethical regulations regarding animal research. *E-selectin* knockout mice were ordered from the Jackson Laboratory (B6.129S4-Sele[tm1/DmiL]) and backcrossed for five generations into the NOD/SCID strain. Genotyping for *E-selectin* knockout was performed as recommended by the Jackson Laboratory. Briefly, ear punches were digested in 75 µl 25 mM NaOH and 0.2 mM EDTA at 95 °C for 20 min, followed by 10 min at 4 °C and neutralization with 75 µl 40 mM Tris–HCl. The PCR reaction mixture contained 2 µl ear-punch digest, 0.2 mM dNTP, 1 µM each primer (5′-aatgtcctatgactcacaggaagcc-3′, 5′-ttctgttcagtggaattgttgttctggcgtt-3′ and 5′-gcagcctctgttccacatacacttc-3′), 1×PCR reaction buffer and 0.5 µl Taq. An annealing temperature of 65 °C was used for 37 cycles followed by 1.5% agarose electrophoresis. The PCR product of WT *SELE* resolves at 182 bp, whereas the mutant resolves at 220 bp. One founder pair of heterozygotes was used to generate homozygous knockout and WT breeder pairs. Age-matched offspring of these breeder pairs were used for xenograft experiments.

All xenograft experiments were conducted on eight-week-old female mice (athymic Nu/Nu, NOD/SCID and NOD/SCID gamma) except in prostate cancer xenografts, which were performed on male mice of the same age. All of the mice were originally ordered from the Jackson Laboratory and breeding was conducted in an specific pathogen-free (SPF) barrier facility. No statistical method was used to predetermine the number of animals needed. Rather, studies in E-selectin WT or knockout SCID mice were performed if the number of age-matched mice per genotype was ≥8. Xenograft experiments were conducted using 50,000 cells suspended in 10 µl PBS for the mammary gland injections or 100,000 cells in 100 µl PBS for the tail vein or intracardiac injections. Bioluminescent imaging was conducted as previously described[26]; however, only bioluminescent signal from the lower third of each mouse was quantified to exclude signal from metastasis in non-bone tissues. Lipopolysaccharide was administered at 0.25 mg per 30 g body mass through intraperitoneal injections 6 h before tissue isolation from eight-week-old WT NOD/SCID mice. Bone marrow was isolated via femur flush, whereas lung tissue was extracted from a single lung lobe. Total RNA quantification by qPCR and statistical comparisons were performed using tissues from the same mouse within the control or lipopolysaccharide conditions. GMI-1271 (Glycomimetics Inc.) was dissolved in PBS at 4 mg ml^{−1} and dosed at 20 mg per kg of body mass twice daily for 14 d immediately following intracardiac injection of BM2 cells. The Wnt inhibitor LF3 (Selleck) was dissolved at 80 mg ml^{−1} in DMSO, diluted to 40 mg ml^{−1} in Cremaphor EL and then diluted in PBS (1:5). The mice were treated at 40 mg kg^{−1} through daily IP injection. Bioluminescence of spontaneous metastasis to the lungs or bones was conducted by retro-orbital injection of luciferin followed by euthanasia, dissection and imaging. The bones or lungs isolated from mice were fixed in 10% buffered formalin or Bouin's solution for 12 h at 22 °C. X-ray images were collected at an exposure of 15 s and 35 keV. The bone lesion counts and areas were calculated manually using ImageJ and a single-blinded review of images. Micro-CT was performed as previously described[63] using core facility-specified threshold values for bone versus non-bone tissues.

Cloning, viral production and transduction. The coding sequence of *Glg1* variants 1 and 3, *Fut3–7* and *Fut9* were cloned from either the complementary DNA of the BM2 cell line or the cDNA of a pooled human reference RNA sample.

Cloned sequences flanked by EcoR1 or Hpa1 restriction sites were inserted into the pMSCV retroviral plasmid. The clones were sequenced and compared with NCBI expressed sequence tags for accuracy. Catalytic mutants of *Fut3* were generated as Glu247Lys (GAG to AAG), Tyr315stop (TAC to TAA) and Gly170Ser (GGC to AGC) according to mutations observed in patients[33,64]. Viral production of Fut enzyme or Glg1 variant pMSCV viruses was performed by transfection into the H29 packaging cell line using polyethylenimine (PEI). The viruses were collected and filtered at 0.45 µm, cells were then transduced using polybrene (8 µg ml^{−1}) for 12 h, followed by culture with 1 µg ml^{−1} puromycin for the duration of the experiments. Dkk1–FLAG was obtained (Addgene, cat. no. 16690) and subcloned into the pLex vector for lentiviral production. Knockdowns were performed using lentiviral shRNA vectors purchased from Sigma (Supplementary Table 7) and knockouts performed using the lentiviral CRISPR–Cas9 vector system pLentiCrispr-v2 (Supplementary Table 7)[65]. Virus was created through PEI transfection of vectors together with the lentiviral packaging plasmids psPax2 and VSVG in 293T cells. Transduction was conducted as described for retroviral plasmids. The SORE6 reporter system[53] used to detect Sox2 transcription by flow cytometry was a gift from L. Wakefield (NCI) and the Wnt reporter system (TGC)[54] used to detect Wnt signalling activation was a gift from R. Nusse (Stanford). Both reporters were inserted into BM2 cells using the described techniques for lentivirus production and delivery. All viral transduction and selection was performed on a cell population-wide basis.

Flow cytometry. For E-selectin binding experiments, a RFP-labelled internal control line and GFP-labelled cells were co-cultured at equal ratios for 48 h; cells were then harvested at 80% confluence by non-enzymatic dissociation buffer (Life Sciences) at 37 °C, washed once with PBS and suspended in flow buffer (10% FBS in PBS supplemented with 1 mM Ca^{2+}/Mg^{2+}) at 1×10^6 cells ml^{−1}. Recombinant mouse E-selectin–IgG Fc or isotype IgG (RD systems) was added at 10 µg ml^{−1} for 1.5 h with vortexing every 15 min. The cells were washed with PBS and incubated with anti-human IgG–AL647-conjugated antibody (BioLegend) at 0.1 µg ml^{−1} for 45 min. The cells were next washed with PBS, resuspended in flow buffer with DAPI (1 µg ml^{−1}) and analysed with the BD LSRII flow cytometer. Internal control cell lines (RFP-labelled) corresponded to the parental population of each cell line—either MDA-MB-231–RFP or SUM159–RFP. The E-selectin binding ratios were quantified using the formula (SELE^{GFP}/IgG^{GFP})/(SELE^{RFP}/IgG^{RFP}). Gating for DAPI, RFP and GFP were performed using negative controls of the corresponding cell line using FlowJo version X. For pharmacological treatments, cells were grown in tunicamycin (Cayman), 1-deoxymannojirimycin (Cayman) or D,L-*three*-PDMP for 24 h. Following differential treatment, internal RFP-labelled cells were added to the cell mixture. For FACS sorting, MDA-MB-231 cells were labelled using this protocol and were sorted into the top and bottom 10% of binding intensities. E-selectin-sorted MDA-MB-231 cells were passaged five times before assessment of the E-selectin binding levels to generate a pool large enough for both flow cytometry and sub-culturing. Negative control treatments (EDTA or GMI-1271) were tested in every cell line to ensure that E-selectin binding was specific. For Wnt signalling activation analysis, BM2 cells stably transduced with the 7×TCF-GFP-SV40-mCherry (TGC) reporter were trypsinized, washed once with PBS and suspended in PBS + 1 µg ml^{−1} DAPI. The cells were analysed with the LSRII instrument and gating analysis was performed using unlabelled BM2 cells using the FlowJo version X software. All flow cytometry experiments were repeated a minimum of three times.

Western blots, qPCR and proliferation assays. Quantitative real-time PCR (qRT–PCR) was performed using the SYBR green mastermix protocol on cDNA generated using the SuperScript III cDNA assembly kit (Invitrogen) and the listed primers (Supplementary Table 7). RNA and DNA were purified using the respective Qiagen kits. Human bone marrow and lung RNA pooled from recently deceased patients was purchased from Takara Bio (cat. nos 636591 and 636531). Western blotting was performed using standard reducing conditions followed by transfer to PVDF membranes. The membranes were blocked in 5% milk in TBS–T, probed with antibodies listed in Supplementary Table 8 and imaged on the Licor Odyssey CLX system using Licor-supplied IRDye680 and IRDye800 secondary antibodies. Anti-Glg1 was detected with the Chemifluorescent substrate kit (Licor). E-selectin immunoprecipitation western blots were performed in the presence of 1 mM CaCl$_2$ for E-selectin–IgG and, along with anti-Slug, were detected with traditional horseradish peroxidase detection. The cell proliferation rates were quantified using the EZQuant reagent (Alstem Bio).

Cell surface protein isolation. Cell surface proteins were biotinylated using the Pierce cell surface protein isolation kit (Thermo Scientific). Briefly, WT and variant M1a cell lines were harvested from two 175 cm^2 flasks by trypsinization, rinsed three times with PBS and suspended in 0.25 mg ml^{−1} solution of Sulfo-NHS-SS-Biotin at 1×10^6 cells ml^{−1} at 4 °C. After 30 min of incubation, 500 µl quenching solution was added to each tube followed by centrifugation at 1,000 r.p.m. for 5 min. The cell pellet was further washed twice in 10 ml Tris-buffered saline. The cell pellets were then lysed with buffer containing 1% NP40. The lysates were equilibrated with NeutrAvidin agarose beads for 2 h at 4 °C. Cell membrane

proteins were eluted by boiling the beads with 100 μl western blot sample buffer with 50 mM DTT for 5 min at 95 °C.

Immunoprecipitation with E-selectin–IgG. M1a cell variants (5×10^6) were harvested from tissue culture flasks and washed three times with PBS. The cell lysates were prepared in Selectin wash/lysis buffer (2% NP40, 150 mM NaCl, 50 mM Tris–HCl (pH 7.4), 2 mM CaCl$_2$, 20 μg ml^{-1} PMSF, and 1×protease inhibitor cocktail (Roche)). The cell lysates were pre-cleared by incubating overnight with Protein G agarose beads (Invitrogen) pre-blocked with BSA. The pre-cleared lysates were then mixed with 10 μg ml^{-1} E-selectin–Ig for 4 h at 4 °C. E-selectin–Ig binding proteins were pulled down via incubation with Protein G agarose beads pre-blocked with BSA and eluted through boiling in 1.5× reducing sample buffer with SDS.

Immunofluorescence. Ex vivo immunofluorescence on bone, lung and liver samples was conducted with or without retro-orbital injection of 10 μg anti-CD31 (Biolegend, cat. no. 102416) in 100 μl PBS to label the vasculature, followed by whole-body perfusion with 10% buffered formalin. The tissues were removed and fixed for 12 h with 10% buffered formalin at 4 °C. These were equilibrated in 15 and 30% sucrose for 3 h each before embedding in SCEM (Section Lab Co) and cryo-sectioning using specialized adhesive film (Section Lab Co). Following evaporation at 22 °C, the sections were fixed for 10 min with buffered formalin, and permeabilized with 20% goat serum and 0.1% Triton X-100 in PBS for 1 h. E-selectin was stained with BV421-conjugated anti-E-selectin (BD Pharmigen, clone 10E9.6; 1:100) for 12 h in 20% goat serum and 0.1% Triton X-100, and the nuclei were counterstained with propidium iodide. Other markers, including EpCam, E-cadherin and Glg1 (Supplementary Table 8), were used similarly except with detection by secondary antibodies and Hoescht counterstaining. The bones of mice injected with cells that expressed endogenous labels (for example, BM2-TGC) were fixed, stained with Hoechst and mounted. Sections were imaged using a standard Nikon A1R confocal point-scanning system. For immunostaining of two clinical samples from patients with prostate cancer bone metastasis, sections from formalin-fixed paraffin-embedded human prostate cancer bone metastasis specimens were dewaxed, rehydrated, treated with Target Retrieval solution (Dako) according to the manufacturer's instructions, blocked with 5% normal donkey serum and incubated for 12 h with anti-E-selectin (R & D Systems, BBA18; 1:50) at 4 °C followed by Alexa Fluor-conjugated secondary antibody (1:300). The sections were then sequentially incubated with anti-Glg1 (Sigma-Aldrich, HPA010815; 1:50) and anti-Ki67 (Dako, M7240; 1:40) using the same procedures. The nuclei were counterstained with DAPI. Images were taken on an Olympus Confocal FV 1000 microscope and representative images from more than ten images per specimen were selected.

Mass spectrometry. The protocol was adapted from previously published work[41] with minor modifications. Substituted reagents include EZLink alkoxyamine-PEG4-Biotin (Thermo), TCEP and chloroacetamide. The metaperiodate concentration was increased to 10 mM. Streptavidin ultralink resin (Pierce) and PNGase F (NEB) were used for isolation. Cells were grown in normal culture conditions and detached with non-enzymatic dissociation buffer. Cells were washed with PBS, suspended in 10 mM sodium metaperiodate at 2×10^6 cells ml^{-1} and rotated at 4 °C for 1 h. The reaction was quenched with 1 mM glycerol, followed by a PBS wash. The cells were resuspended in 100 μM EZLink alkoxyamine-PEG4-biotin supplemented with 10 mM aniline in PBS + 5% FBS followed by rotation at 4 °C for 1 h. The cells were then washed with PBS and either conjugated with Streptavidin–AL647 (Biolegend; 10 μg ml^{-1}) for verification of efficient oxidation and conjugation by flow cytometry/microscopy or lysed (1% Triton X-100, 150 mM NaCl, 1×protease inhibitor, 5 mM chloroacetimide, 0.1 mg ml^{-1} PMSF and 10 mM Tris–HCl, pH 7.6) at 10^6 cells ml^{-1} end-over-end at 4 °C for 30 min. The supernatants were saved after sequential centrifugation at 2,800g and 16,000g. The supernatants were then incubated with 6 μl washed resin per 10^6 cells at 4 °C for 12 h. Beads were washed 10× each with lysis buffer and 0.5% SDS in PBS. The beads were next incubated in 0.5% SDS in PBS, 50 mM TCEP for 20 min at 22 °C, washed 10× with 6 M urea in 100 mM Tris–HCl pH 8.5, then incubated with 6 M urea in 100 mM Tris–HCl (pH 8.5) and 50 mM chloroacetamide for 20 min. The beads were then washed 10× with each of the following: 6 M urea in 100 mM Tris–HCl pH 8.5, 5 M NaCl, 100 mM sodium carbonate, PBS and water. The beads were subsequently digested with 5 μg sequencing-grade trypsin in 0.5 ml ammonium bicarbonate at 37 °C for 24 h. Tryptic peptides were isolated by centrifugation and one wash with ammonium bicarbonate. Finally, the beads were washed 10× each with PBS and water, and digested with 2,500 U PNGase F in glycobuffer 2 (NEB) for 10 h at 37 °C. The supernatant and the first wash were pooled for mass spectrometry. The peptides released by PNGase F digestion were identified by nanoscale liquid chromatography–tandem mass spectrometry using a previously described method[66]. The Skyline software was used for the relative quantification of peptides by calculating the peptide peak areas from MS1-extracted ion chromatograms, as previously described[67]. The total protein characterization is listed in Supplementary Table 2.

E-selectin plate coating and immunofluorescence. Ibidi culture-treated chamber slides were coated with E-selectin–Fc chimera at 10 μg ml^{-1} in PBS for 12 h at

4 °C. Indirect immunofluorescence for markers of MET was conducted by fixing cells that were grown for 24 h in coated Ibidi chamber slides with 10% buffered formalin solution for 20 min at 4 °C, followed by permeabilization with 0.1% Triton X-100 in PBS and incubation with each antibody for 12 h at 4 °C. N-cadherin (BD Pharmigen, cat. no. 610920), ZO-1 (CST, cat. no. 5406), EpCam (CST, clone VU1D9) and K14 (Biolegend, cat. no. 905301) were used at dilutions of 1:100 for immunofluorescence. The slides were washed with PBS, Hoechst and probed with the appropriate secondary antibodies (Invitrogen), followed by confocal imaging of chambers filled with PBS. Wnt activation by live cell imaging of BM2-TGC seeded over E-selectin in Ibidi culture slides was conducted from 0–48 h through total internal reflectance fluorescence microscopy and was first observable approximately 30 h post seeding. Analysis of Wnt activation by flow cytometry was conducted at 48 h. The cells analysed by flow cytometry were trypsinized, centrifuged and immediately analysed using DAPI as a cell-death indicator. Various inducers and inhibitors of Wnt signalling were added to the culture, these include ICG-001 (Selleck; 25 μM), LF3 (Selleck; 50 μM), Wnt3a- or control-conditioned media and recombinant Wnt3a (RD systems; 100 ng ml^{-1}). Wnt3a and control-conditioned media were generated by collecting 72-h-conditioned media from L cells with or without Wnt3a expression (ATCC, CRL-2647 and CRL-2648) followed by filtration at 0.45 μm.

Microarray analysis. BM2 and M1a cells were seeded over 6 cm tissue-culture-treated plates coated with E-selectin–IgG or control IgG (10 μg ml^{-1}) for 12 h at 37 °C. RNA was isolated from cells using the RNAeasy minikit (Qiagen) according to manufacturer's instructions. Gene expression profiles influenced by E-selectin binding were analysed using the Agilent human GE 8×60K two-colour microarray system (Agilent, G4858A-039494). Briefly, the RNA samples and a universal human reference RNA (Agilent) were labelled with CTP-cy5 and CTP-cy3 using the Agilent Quick Amp labelling kit. Labelled samples were mixed equally and hybridized to the array. The array was then scanned with the G2505C scanner (Agilent). Data was deconvoluted and analysed with the Genespring v13 software (Agilent). Briefly, array controls, flagged values and expression values falling below the median value were removed. Multiple values for any given gene were collapsed into the single highest expression value. Data was extracted as a log$_2$-transformed ratio of Cy5/Cy3.

GSEA. Data that was log$_2$transformed was subtracted (log$_2$[E-selectin]−log$_2$[IgG]) and rank ordered for each cell line. The data was analysed using GSEAv2.0. Interrogated signatures from the MySigDB v5.1 database included the Hallmark EMT dataset (M5930), Sarrio-EMT (GSE8430), Claudin-low (GSE18229), Luminal (GSE22446), Bruno-hematopoiesis (M1492) and Blick-EMT[68] as part of a broader, manually compiled set of EMT- and Stem cell-related signatures. Only data sets with a nominal $P < 0.05$ were considered in the analysis.

Statistics and reproducibility. All statistical comparisons were conducted with Stata v13 (Mann–Whitney U and Cox's proportional hazards), Microsoft Excel 2010 (t-test) and Broad Institute GSEA software (pre-ranked GSEA analysis). Results are reported as mean ± s.e.m. for the bar graphs. For all animal experiments, animals were only excluded if they died or had to be sacrificed according to the pre-defined criteria listed in the IACUC protocol. A two-sided Mann–Whitney U test was used for bone metastasis as this data does not exhibit a normal distribution. Osteolytic area and lesion analyses assumed each hindlimb as an independent event. Bioluminescent data from the imaging of spontaneous bone metastasis in the Fut primary tumour injection or Ob1 bone metastasis experiments were set to zero for values below a threshold of 100,000 ph s^{-1} or by visual inspection to avoid false ranking attributed only to background signal. For spontaneous bone and lung metastasis from M1a–Fut cells, one-sided Mann–Whitney U and one-sided Fisher's exact tests were used to test whether Fut overexpression promoted spontaneous metastasis to bone, whereas theone-sided Student's t-test was used to assess whether Fut expression promoted lung metastasis. Two-sided, unpaired Student's t-tests were used for all other lung metastasis, primary tumour growth, qPCR, flow cytometry and other normal data. All statistical comparisons are non-significant at an alpha level of 0.05 if not marked by a specific P value. Patient expression values in the NKI-295 and EMC-MSK datasets were stratified by median value for single gene analysis or grouped by median-stratified values according to Glg1 and Fut3 or Fut6. The log$_2$[reads per kilobase of transcript per million mapped reads] values of exon1 from each Fut gene were extracted from the TCGA dataset and plotted. Survival data for the mouse experiments and patient datasets were analysed by the Cox's proportional hazards model to generate hazard ratios and their associated P values. All in vivo bone metastasis experiments were performed at least two times to ensure reproducibility and significance with the exception of the BM2-CD44-KO injection, catalytic Fut3 mutants and GMI-1271 treatment experiments, which were performed once. All lung metastasis and primary tumour growth experiments were performed once. All other experiments were repeated according to their corresponding figure legends with similar results.

Reporting Summary. Further information on research design is available in the Nature Research Reporting Summary linked to this article.

Data availability

The microarray data that support the findings of this study have been deposited in the Gene Expression Omnibus (GEO) under the accession code GSE96754 and the mass spectrometry proteomics data have been deposited to the ProteomeXchange Consortium via the PRIDE partner repository with the dataset identifier PXD012942; the mass spectrometry data is further available in Supplementary Table 2. The human clinical breast cancer data are not available in GEO; these were derived from the TCGA Research Network and the dataset derived from this resource that supports the findings of this study is available in https://xenabrowser.net/datapages/?cohort=GDC%20TCGA%20Breast%20Cancer%20(BRCA). The human breast cancer data were also derived from the NKI-295 dataset[17], which is available at https://xenabrowser.net/datapages/?cohort=Breast%20Cancer%20. Finally, the human breast cancer data from the EMC-MSK dataset is available in the publication by Bos and colleagues[69]. The source data relevant for the clinical data analyses performed in this study are available in Supplementary Table 9. Unprocessed western blot images are provided as Supplementary Fig. 9. The source data supporting the findings of this study are provided in Supplementary Table 9. All protocols, cell lines and reagents are available from the corresponding author on request.

References

62. Forozan, F. et al. Molecular cytogenetic analysis of 11 new breast cancer cell lines. *Br. J. Cancer* **81**, 1328–1334 (1999).
63. Ell, B. et al. Tumor-induced osteoclast miRNA changes as regulators and biomarkers of osteolytic bone metastasis. *Cancer Cell* **24**, 542–556 (2013).
64. Koda, Y., Kimura, H. & Mekada, E. Analysis of Lewis fucosyltransferase genes from the human gastric mucosa of Lewis-positive and -negative individuals. *Blood* **82**, 2915–2919 (1993).
65. Sanjana, N. E., Shalem, O. & Zhang, F. Improved vectors and genome-wide libraries for CRISPR screening. *Nat. Methods* **11**, 783–784 (2014).
66. Diner, B. A. et al. The functional interactome of PYHIN immune regulators reveals IFIX is a sensor of viral DNA. *Mol. Syst. Biol.* **11**, 787 (2015).
67. Giguere, S. S. et al. The proteomic profile of deleted in breast cancer 1 (DBC1) interactions points to a multifaceted regulation of gene expression. *Mol. Cell. Proteomics* **15**, 791–809 (2016).
68. Blick, T. et al. Epithelial mesenchymal transition traits in human breast cancer cell lines parallel the CD44hi/CD24lo/- stem cell phenotype in human breast cancer. *J. Mammary Gland Biol. Neoplasia* **15**, 235–252 (2010).
69. Bos, P. D. et al. Genes that mediate breast cancer metastasis to the brain. *Nature* **459**, 1005–1009 (2009).

nature research

Corresponding author(s): Yibin Kang

Last updated by author(s): Mar 4, 2019

Reporting Summary

Nature Research wishes to improve the reproducibility of the work that we publish. This form provides structure for consistency and transparency in reporting. For further information on Nature Research policies, see Authors & Referees and the Editorial Policy Checklist.

Statistics

For all statistical analyses, confirm that the following items are present in the figure legend, table legend, main text, or Methods section.

n/a	Confirmed	
☐	☒	The exact sample size (*n*) for each experimental group/condition, given as a discrete number and unit of measurement
☐	☒	A statement on whether measurements were taken from distinct samples or whether the same sample was measured repeatedly
☐	☒	The statistical test(s) used AND whether they are one- or two-sided *Only common tests should be described solely by name; describe more complex techniques in the Methods section.*
☒	☐	A description of all covariates tested
☐	☒	A description of any assumptions or corrections, such as tests of normality and adjustment for multiple comparisons
☐	☒	A full description of the statistical parameters including central tendency (e.g. means) or other basic estimates (e.g. regression coefficient) AND variation (e.g. standard deviation) or associated estimates of uncertainty (e.g. confidence intervals)
☒	☐	For null hypothesis testing, the test statistic (e.g. *F*, *t*, *r*) with confidence intervals, effect sizes, degrees of freedom and *P* value noted *Give P values as exact values whenever suitable.*
☒	☐	For Bayesian analysis, information on the choice of priors and Markov chain Monte Carlo settings
☒	☐	For hierarchical and complex designs, identification of the appropriate level for tests and full reporting of outcomes
☒	☐	Estimates of effect sizes (e.g. Cohen's *d*, Pearson's *r*), indicating how they were calculated

Our web collection on statistics for biologists contains articles on many of the points above.

Software and code

Policy information about availability of computer code

Data collection	Data was collected using standard software programs including: Nikon Elements for microscopy, FlowJo v10 and FACSDiva for flow cytometry, Licor Odyssey Clx for western blot, ImageJ for bone metastasis x-rays, LivingImage for bioluminescence, Skyline for Mass spectrometry, Genespring v13 for microarray, and GSEA-BroadInstitute for GSEA analysis. These have mentioned in the text where its reporting is customarily used. Stata and Excel were used for basic data display and statistical tests. No code was used to collect any data.
Data analysis	Excel functions ttest and stdev used for Student's T-test and standard deviation calculations. Stata ranksum used for Mann-Whitney U test and stcox used for Cox's Proportional Hazards model. Vioplot add-in used for stata graphing of violin plots. GSEA pre-ranked GSEA used for GSEA analysis.

For manuscripts utilizing custom algorithms or software that are central to the research but not yet described in published literature, software must be made available to editors/reviewers. We strongly encourage code deposition in a community repository (e.g. GitHub). See the Nature Research guidelines for submitting code & software for further information.

Data

Policy information about availability of data

All manuscripts must include a data availability statement. This statement should provide the following information, where applicable:
- Accession codes, unique identifiers, or web links for publicly available datasets
- A list of figures that have associated raw data
- A description of any restrictions on data availability

Microarray data that support the findings of this study have been deposited in the Gene Expression Omnibus (GEO) under accession codes GSE96754, and the mass spectrometry proteomics data have been deposited to the ProteomeXchange Consortium via the PRIDE partner repository with the dataset identifier PXD012942; mass spectrometry data is further available in Supplementary Table 2.
The human clinical breast cancer data are not available in GEO; these were derived from the TCGA Research Network and the data-set derived from this resource that supports the findings of this study is available in https://xenabrowser.net/datapages/?cohort=GDC%20TCGA%20Breast%20Cancer%20(BRCA)
The human breast cancer data were also derived from the NKI-295 dataset which is available at https://xenabrowser.net/datapages/?cohort=Breast%20Cancer%

20(Vijver%202002)
Finally, human breast cancer data from the EMC-MSK dataset is available in Bos et. al, 2009. Source data relevant for the clinical data analyses performed in this study are available in Supplementary Table 9.

Field-specific reporting

Please select the one below that is the best fit for your research. If you are not sure, read the appropriate sections before making your selection.

☒ Life sciences ☐ Behavioural & social sciences ☐ Ecological, evolutionary & environmental sciences

For a reference copy of the document with all sections, see nature.com/documents/nr-reporting-summary-flat.pdf

Life sciences study design

All studies must disclose on these points even when the disclosure is negative.

Sample size	For most experiments, biological replicates and/or technical repeats were included and most experiments were repeated at least 3 times. Such sample sizes are typical of the in vitro experiments (e.g. qRT-PCR) used in the study. For in vivo experiments, sample size of n = 8-10 are typical of experiments and are used in the study, but this number varies according to the number of wild-type and knockout mice per litter in the E-selectin knockout experiment or when the number of mice in a single experiment was >40 animals. No sample size calculation was performed to predetermine sample size. All sample sizes are listed in the corresponding figure legend.
Data exclusions	Animals were excluded only if they died or had to be sacrificed because of moribund conditions specified in the IACUC protocol. Such events occurred in less than 5% of animals during the experimental time frame. This exclusion criteria was pre-determined by the protocol.
Replication	Immunofluorescence, western blot, mass spectrometry controls, flow cytometry and E-selectin plate-binding assays were conducted ≥3 times to ensure reproducibility unless otherwise noted. All in vivo bone metastasis experiments were performed at least 2 times to ensure reproducibility and significance with the exception of the BM2-CD44 KO injection, catalytic Fut3 mutants and the GMI-1271 treatment, which was performed once. All lung metastasis and primary tumor growth experiments were performed once with appropriate group size and statistics. All attempts at replication were successful.
Randomization	Standard mice (Nu/Nu or NSG) for xenograft experiments were randomized, with each group receiving an equal number of mice from each litter. E-selectin knockout compared to wild-type mice were not randomized, rather, every available mouse within 20 days of the same date of birth was used.
Blinding	No blinding was performed with the exception of x-ray analysis and quantification. In this case, the investigator was blinded to the experimental group of each x-ray. For all other cases, blinding was not relevant to the experiment as the results were directly collected by instrumentation.

Behavioural & social sciences study design

All studies must disclose on these points even when the disclosure is negative.

Study description	*Briefly describe the study type including whether data are quantitative, qualitative, or mixed-methods (e.g. qualitative cross-sectional, quantitative experimental, mixed-methods case study).*
Research sample	*State the research sample (e.g. Harvard university undergraduates, villagers in rural India) and provide relevant demographic information (e.g. age, sex) and indicate whether the sample is representative. Provide a rationale for the study sample chosen. For studies involving existing datasets, please describe the dataset and source.*
Sampling strategy	*Describe the sampling procedure (e.g. random, snowball, stratified, convenience). Describe the statistical methods that were used to predetermine sample size OR if no sample-size calculation was performed, describe how sample sizes were chosen and provide a rationale for why these sample sizes are sufficient. For qualitative data, please indicate whether data saturation was considered, and what criteria were used to decide that no further sampling was needed.*
Data collection	*Provide details about the data collection procedure, including the instruments or devices used to record the data (e.g. pen and paper, computer, eye tracker, video or audio equipment) whether anyone was present besides the participant(s) and the researcher, and whether the researcher was blind to experimental condition and/or the study hypothesis during data collection.*
Timing	*Indicate the start and stop dates of data collection. If there is a gap between collection periods, state the dates for each sample cohort.*
Data exclusions	*If no data were excluded from the analyses, state so OR if data were excluded, provide the exact number of exclusions and the rationale behind them, indicating whether exclusion criteria were pre-established.*
Non-participation	*State how many participants dropped out/declined participation and the reason(s) given OR provide response rate OR state that no participants dropped out/declined participation.*

Randomization	*If participants were not allocated into experimental groups, state so OR describe how participants were allocated to groups, and if allocation was not random, describe how covariates were controlled.*

Ecological, evolutionary & environmental sciences study design

All studies must disclose on these points even when the disclosure is negative.

Study description	*Briefly describe the study. For quantitative data include treatment factors and interactions, design structure (e.g. factorial, nested, hierarchical), nature and number of experimental units and replicates.*
Research sample	*Describe the research sample (e.g. a group of tagged Passer domesticus, all Stenocereus thurberi within Organ Pipe Cactus National Monument), and provide a rationale for the sample choice. When relevant, describe the organism taxa, source, sex, age range and any manipulations. State what population the sample is meant to represent when applicable. For studies involving existing datasets, describe the data and its source.*
Sampling strategy	*Note the sampling procedure. Describe the statistical methods that were used to predetermine sample size OR if no sample-size calculation was performed, describe how sample sizes were chosen and provide a rationale for why these sample sizes are sufficient.*
Data collection	*Describe the data collection procedure, including who recorded the data and how.*
Timing and spatial scale	*Indicate the start and stop dates of data collection, noting the frequency and periodicity of sampling and providing a rationale for these choices. If there is a gap between collection periods, state the dates for each sample cohort. Specify the spatial scale from which the data are taken*
Data exclusions	*If no data were excluded from the analyses, state so OR if data were excluded, describe the exclusions and the rationale behind them, indicating whether exclusion criteria were pre-established.*
Reproducibility	*Describe the measures taken to verify the reproducibility of experimental findings. For each experiment, note whether any attempts to repeat the experiment failed OR state that all attempts to repeat the experiment were successful.*
Randomization	*Describe how samples/organisms/participants were allocated into groups. If allocation was not random, describe how covariates were controlled. If this is not relevant to your study, explain why.*
Blinding	*Describe the extent of blinding used during data acquisition and analysis. If blinding was not possible, describe why OR explain why blinding was not relevant to your study.*

Did the study involve field work? ☐ Yes ☐ No

Field work, collection and transport

Field conditions	*Describe the study conditions for field work, providing relevant parameters (e.g. temperature, rainfall).*
Location	*State the location of the sampling or experiment, providing relevant parameters (e.g. latitude and longitude, elevation, water depth).*
Access and import/export	*Describe the efforts you have made to access habitats and to collect and import/export your samples in a responsible manner and in compliance with local, national and international laws, noting any permits that were obtained (give the name of the issuing authority, the date of issue, and any identifying information).*
Disturbance	*Describe any disturbance caused by the study and how it was minimized.*

Reporting for specific materials, systems and methods

We require information from authors about some types of materials, experimental systems and methods used in many studies. Here, indicate whether each material, system or method listed is relevant to your study. If you are not sure if a list item applies to your research, read the appropriate section before selecting a response.

Materials & experimental systems

n/a	Involved in the study
☐	☒ Antibodies
☐	☒ Eukaryotic cell lines
☒	☐ Palaeontology
☐	☒ Animals and other organisms
☒	☐ Human research participants
☒	☐ Clinical data

Methods

n/a	Involved in the study
☒	☐ ChIP-seq
☐	☒ Flow cytometry
☒	☐ MRI-based neuroimaging

Antibodies

Antibodies used	Glg1 (Sigma HPA010815, 1:1000-IB or 1:100 IF), CD44 (Cell Signaling Technologies clone 156-3C11, 1:1000), Beta-actin (Santa Cruz sc47778, 1:1000), N-cadherin (BD Pharmigen 610920, clone 32, 1:1000-IB, 1:100 IF), FLAG (Sigma F7425, 1:1000), Fut3 (Abcam ab110082, 1:1000), E-selectin (BD Pharmigen clone 109.E6, 1:100), EpCam (CST VU1D9, 1:100), E-cadherin (BD Pharmigen 610181, clone 10E9.6, 1:100), Ki67 (Dako M7240, clone MIB-1, 1:40), ZO-1 (CST 5406, 1:100), EpCAM (CST VU1D9, 1:100), K14 (Biolegend 905301, 1:100), Slug (Santa Cruz clone A-7, 1:50), E-selectin (R&D systems BBA18, 1:50), Glg1 (Personal gift, Charles Dimitroff, 1:1000). This data is available in Supplementary Table 8.
	All secondary antibodies used were Licor IRDye 680/800 anti-rabbit or anti-mouse for western blot (925-322#, 1:10000), Dako polyclonal anti-rabbit or anti-mouse-HRP for western blot (P0448, 1:2000) or Invitrogen AL555 or AL647 anti-rabbit or anti-mouse (e.g. A-21244, 1:1000) for immunofluorescence.
Validation	All commercial antibodies were validated by the manufacturer for the species and application used in this study. Glg1, CD44, Fut3, and FLAG antibodies were validated for western blot via specific knockout or overexpression followed by western blotting- data for each is displayed in the manuscript. All bands appeared at the correct apparent molecular weight. Beta-actin, Slug, CD31, EpCam, E-cadherin, K-14, Ki-67 antibodies were previously validated in our lab for the intended species and application used here. E-selectin and Glg1 antibodies were validated for IF by overexpression in HEK-293T cells followed by indirect immunofluorescence. In addition, all antibodies used here have been validated by reviews on Biocompare. anti-Glg1 from Charles Dimitroff has been previously validated by Robert Sackstein's laboratory and was furthermore validated in this study by specific knockout and overexpression of Glg1 followed by western blotting in Supplementary Fig. 5.

Eukaryotic cell lines

Policy information about cell lines

Cell line source(s)	Key characteristics of each cell line, including source, are included in Supplementary table 1. The MDA-MB-231 cells and its derivatives (SCP6, SCP32, SCP28, SCP2, SCP25, LM2, BM2) were from Joan Massague's lab. SUM159 was from Stephen Ethier's lab at the Karmanos Institute and the derivatives were made by this study's lead author. DU145 was obtained from ATCC and the ob1 bone-metastatic derivatives were generated by this study's lead author. L Cells were obtained from ATCC. PCR1 cell line was obtained from Steven Barthel.
Authentication	All cell lines were authenticated by STR profiling with a similarity score >90%.
Mycoplasma contamination	All cells were tested for mycoplasma infection either upon derivation and freezing or after 1 month of culture via PCR testing. All cultures were confirmed negative and no instances of mycoplasma contamination occurred throughout the study period.
Commonly misidentified lines (See ICLAC register)	No cell lines used in this study were found in the database of commonly misidentified cell lines that is maintained by ICLAC and NCBI Biosample.

Palaeontology

Specimen provenance	*Provide provenance information for specimens and describe permits that were obtained for the work (including the name of the issuing authority, the date of issue, and any identifying information).*
Specimen deposition	*Indicate where the specimens have been deposited to permit free access by other researchers.*
Dating methods	*If new dates are provided, describe how they were obtained (e.g. collection, storage, sample pretreatment and measurement), where they were obtained (i.e. lab name), the calibration program and the protocol for quality assurance OR state that no new dates are provided.*

☐ Tick this box to confirm that the raw and calibrated dates are available in the paper or in Supplementary Information.

Animals and other organisms

Policy information about studies involving animals; ARRIVE guidelines recommended for reporting animal research

Laboratory animals	E-selectin knockout mice were ordered from the Jackson Laboratory (B6.129S4-Seletm1/DmiL) and were backcrossed for 5 generations into the NOD/SCID strain. All xenograft experiments were conducted on 8 week old female mice (athymic Nu/Nu, NOD/SCID, NOD/SCID Gamma) except in prostate cancer xenografts, which were performed on male mice of the same age. All mice were originally ordered from the Jackson Laboratory and breeding was conducted in an SPF barrier facility.
Wild animals	The study did not use wild animals.
Field-collected samples	The study did not use field-collected samples.
Ethics oversight	All procedures involving mice and experimental protocols were approved by the University Institutional Animal Care and Use Committee (IACUC).

Note that full information on the approval of the study protocol must also be provided in the manuscript.

Human research participants

Policy information about studies involving human research participants

Population characteristics	*Describe the covariate-relevant population characteristics of the human research participants (e.g. age, gender, genotypic information, past and current diagnosis and treatment categories). If you filled out the behavioural & social sciences study design questions and have nothing to add here, write "See above."*
Recruitment	*Describe how participants were recruited. Outline any potential self-selection bias or other biases that may be present and how these are likely to impact results.*
Ethics oversight	*Identify the organization(s) that approved the study protocol.*

Note that full information on the approval of the study protocol must also be provided in the manuscript.

Clinical data

Policy information about clinical studies

All manuscripts should comply with the ICMJE guidelines for publication of clinical research and a completed CONSORT checklist must be included with all submissions.

Clinical trial registration	*Provide the trial registration number from ClinicalTrials.gov or an equivalent agency.*
Study protocol	*Note where the full trial protocol can be accessed OR if not available, explain why.*
Data collection	*Describe the settings and locales of data collection, noting the time periods of recruitment and data collection.*
Outcomes	*Describe how you pre-defined primary and secondary outcome measures and how you assessed these measures.*

ChIP-seq

Data deposition

☐ Confirm that both raw and final processed data have been deposited in a public database such as GEO.

☐ Confirm that you have deposited or provided access to graph files (e.g. BED files) for the called peaks.

Data access links *May remain private before publication.*	*For "Initial submission" or "Revised version" documents, provide reviewer access links. For your "Final submission" document, provide a link to the deposited data.*
Files in database submission	*Provide a list of all files available in the database submission.*
Genome browser session (e.g. UCSC)	*Provide a link to an anonymized genome browser session for "Initial submission" and "Revised version" documents only, to enable peer review. Write "no longer applicable" for "Final submission" documents.*

Methodology

Replicates	*Describe the experimental replicates, specifying number, type and replicate agreement.*
Sequencing depth	*Describe the sequencing depth for each experiment, providing the total number of reads, uniquely mapped reads, length of reads and whether they were paired- or single-end.*
Antibodies	*Describe the antibodies used for the ChIP-seq experiments; as applicable, provide supplier name, catalog number, clone name, and lot number.*
Peak calling parameters	*Specify the command line program and parameters used for read mapping and peak calling, including the ChIP, control and index files used.*
Data quality	*Describe the methods used to ensure data quality in full detail, including how many peaks are at FDR 5% and above 5-fold enrichment.*
Software	*Describe the software used to collect and analyze the ChIP-seq data. For custom code that has been deposited into a community repository, provide accession details.*

Flow Cytometry

Plots

Confirm that:

☒ The axis labels state the marker and fluorochrome used (e.g. CD4-FITC).

☒ The axis scales are clearly visible. Include numbers along axes only for bottom left plot of group (a 'group' is an analysis of identical markers).

☒ All plots are contour plots with outliers or pseudocolor plots.

☒ A numerical value for number of cells or percentage (with statistics) is provided.

Methodology

Sample preparation	For E-selectin binding experiments, RFP- and GFP-labeled cells were co-cultured at equal ratios for 48 h, then cells were harvested at 80% confluence by non-enzymatic dissociation buffer (Life Sciences) at 37°C, washed once with PBS, and suspended in flow buffer (10% FBS in PBS supplemented with 1 mM Ca2+/Mg2+) at 1 million cells/mL. Recombinant mouse E-selectin/ IgG Fc or Isotype IgG (RD systems) was added at 10 ug/mL for 1.5 h with vortexing every 15 min. Cells were washed with PBS and incubated with anti-human IgG-AL647-conjugated antibody (Biolegend) at 0.1ug/mL for 45 min. Cells were washed with PBS, resuspended in flow buffer with DAPI (1 ug/mL), and analyzed with the BD LSRII flow cytometer. Internal control cell lines (RFP-labeled) corresponded to the parental population of each cell line – either MDA-MB-231-RFP or SUM159-RFP. E-selectin binding ratios were quantified using the formula (SELEGFP/IgGGFP)/(SELERFP/IgGRFP). Gating for DAPI, RFP, and GFP were performed using negative controls of the corresponding cell line using FlowJo version X. For pharmacological, cells were grown in Tunicamycin, Deoxymannojirimycin, or PDMP for 48h. Following differential treatment, internal control RFP-labeled cells were added to the cell mixture. For FACS sorting, MDA-MB-231 cells were labeled using this protocol and were sorted into the top and bottom 10% of binding intensities. E-selectin-sorted MDA-MB-231 cells were passaged 5 times prior to assessing E-selectin binding levels to generate a large enough pool both for flow cytometry and sub-culturing. Negative control treatments (EDTA or GMI-1271) were tested in every cell line to ensure that E-selectin binding was specific. For Wnt signaling activation analysis, BM2 cells stably transduced with the 7x-TCF-GFP-SV40-mCherry (TGC) reporter were trypsinized, washed once with PBS, and suspended in PBS + 1 ug/mL DAPI. Cells were analyzed with the LSRII instrument, and gating analysis was performed using unlabeled BM2 cells using the FlowJo version X software. All flow cytometry experiments were repeated a minimum of three times.
Instrument	BD LSRII
Software	FACSDiva and FlowJo Version X were used to set gates and collect data.
Cell population abundance	No cell sorting was performed beyond isolating the top and bottom deciles for the E-selectin-sorted cell lines.
Gating strategy	FSC and SSC gates were set to include at least 90% of events and to exclude very small events. SSC-A and -H or FSC-A and -H were used to discriminate for only single cells. DAPI or PI were used to discriminate live cells from dead using appropriate negative and positive controls. GFP and RFP gating was performed using negative controls from the respective cell lines tested, or from using appropriate internal controls (I.e. the Sore6 reporter system which used a control plasmid to control for endogenous mCherry transcription) such that the negative control sample showed no more than 1% positivity. All binding analyses were performed using an internal control to control for differences in cell culture, harvesting or probing conditions. This internal control was used to normalize all experiments as described.

☒ Tick this box to confirm that a figure exemplifying the gating strategy is provided in the Supplementary Information.

Magnetic resonance imaging

Experimental design

Design type	*Indicate task or resting state; event-related or block design.*
Design specifications	*Specify the number of blocks, trials or experimental units per session and/or subject, and specify the length of each trial or block (if trials are blocked) and interval between trials.*
Behavioral performance measures	*State number and/or type of variables recorded (e.g. correct button press, response time) and what statistics were used to establish that the subjects were performing the task as expected (e.g. mean, range, and/or standard deviation across subjects).*

Acquisition

Imaging type(s)
Specify: functional, structural, diffusion, perfusion.

Field strength
Specify in Tesla

Sequence & imaging parameters
Specify the pulse sequence type (gradient echo, spin echo, etc.), imaging type (EPI, spiral, etc.), field of view, matrix size, slice thickness, orientation and TE/TR/flip angle.

Area of acquisition
State whether a whole brain scan was used OR define the area of acquisition, describing how the region was determined.

Diffusion MRI ☐ Used ☐ Not used

Preprocessing

Preprocessing software
Provide detail on software version and revision number and on specific parameters (model/functions, brain extraction, segmentation, smoothing kernel size, etc.).

Normalization
If data were normalized/standardized, describe the approach(es): specify linear or non-linear and define image types used for transformation OR indicate that data were not normalized and explain rationale for lack of normalization.

Normalization template
Describe the template used for normalization/transformation, specifying subject space or group standardized space (e.g. original Talairach, MNI305, ICBM152) OR indicate that the data were not normalized.

Noise and artifact removal
Describe your procedure(s) for artifact and structured noise removal, specifying motion parameters, tissue signals and physiological signals (heart rate, respiration).

Volume censoring
Define your software and/or method and criteria for volume censoring, and state the extent of such censoring.

Statistical modeling & inference

Model type and settings
Specify type (mass univariate, multivariate, RSA, predictive, etc.) and describe essential details of the model at the first and second levels (e.g. fixed, random or mixed effects; drift or auto-correlation).

Effect(s) tested
Define precise effect in terms of the task or stimulus conditions instead of psychological concepts and indicate whether ANOVA or factorial designs were used.

Specify type of analysis: ☐ Whole brain ☐ ROI-based ☐ Both

Statistic type for inference
(See Eklund et al. 2016)
Specify voxel-wise or cluster-wise and report all relevant parameters for cluster-wise methods.

Correction
Describe the type of correction and how it is obtained for multiple comparisons (e.g. FWE, FDR, permutation or Monte Carlo).

Models & analysis

n/a | Involved in the study
☐ | ☐ Functional and/or effective connectivity
☐ | ☐ Graph analysis
☐ | ☐ Multivariate modeling or predictive analysis

Functional and/or effective connectivity
Report the measures of dependence used and the model details (e.g. Pearson correlation, partial correlation, mutual information).

Graph analysis
Report the dependent variable and connectivity measure, specifying weighted graph or binarized graph, subject- or group-level, and the global and/or node summaries used (e.g. clustering coefficient, efficiency, etc.).

Multivariate modeling and predictive analysis
Specify independent variables, features extraction and dimension reduction, model, training and evaluation metrics.